Natural Resources Canada | Ressources naturelles Canada

GEOLOGICAL SURVEY OF CANADA
OPEN FILE 8563

# Till composition across the Keewatin Ice Divide in the Tehery-Wager GEM-2 Rae project area, Nunavut

I. McMartin, I. Randour, and N. Wodicka

2019

Canada

**GEOLOGICAL SURVEY OF CANADA**
**OPEN FILE 8563**

# Till composition across the Keewatin Ice Divide in the Tehery-Wager GEM-2 Rae project area, Nunavut


## I. McMartin[1], I. Randour[2], and N. Wodicka[1]

[1] Geological Survey of Canada, 601 Booth Street Ottawa, Ontario K1A 0E8
[2] Université du Québec à Montréal (UQÀM), 405 Rue Sainte-Catherine Est, Montréal, Québec H2L 2C4


## 2019


© Her Majesty the Queen in Right of Canada, as represented by the Minister of Natural Resources, 2019

Information contained in this publication or product may be reproduced, in part or in whole, and by any means, for personal or public non-commercial purposes, without charge or further permission, unless otherwise specified.
You are asked to:
- exercise due diligence in ensuring the accuracy of the materials reproduced;
- indicate the complete title of the materials reproduced, and the name of the author organization; and
- indicate that the reproduction is a copy of an official work that is published by Natural Resources Canada (NRCan) and that the reproduction has not been produced in affiliation with, or with the endorsement of, NRCan.

Commercial reproduction and distribution is prohibited except with written permission from NRCan. For more information, contact NRCan at nrcan.copyrightdroitdauteur.rncan@canada.ca.



Permanent link: https://doi.org/10.4095/314707

This publication is available for free download through GEOSCAN (https://geoscan.nrcan.gc.ca/).

**Recommended citation**
McMartin, I., Randour, I., and Wodicka, N., 2019. Till composition across the Keewatin Ice Divide in the Tehery-Wager GEM-2 Rae project area, Nunavut; Geological Survey of Canada, Open File 8563, 1 .zip file. https://doi.org/10.4095/314707

Publications in this series have not been edited; they are released as submitted by the author.

## TABLE OF CONTENTS



**Appendices**

The Readme file provides the complete list of files and sub-directories containing the datasets:

1. Field site location and description
2. Ice-flow indicator location and description
3. Sample location and description
4. Till geochemistry, <0.063 mm
5. Till matrix color and sand-silt-clay distribution
6. Till matrix carbon and LOI contents, <0.063 mm
7. X-Ray diffraction analyses, <0.002 mm
8. Till pebble counts, 8-30 mm, % counted
9. Gold grain and indicator mineral counts (0.25-2 mm)
10. Electron microprobe analyses
11. Metadata

**List of figures**



**List of table**

## ABSTRACT

This report releases the field database and analytical results from a targeted surficial geology and till sampling survey completed in 2015 and 2016 south of Wager Bay in mainland Nunavut as part of Natural Resources Canada's Tehery-Wager GEM-2 Rae project. The report also provides a summary of the regional bedrock and surficial geology, an improved glacial history framework, and a detailed description of the field and analytical methods. A preliminary interpretation regarding till provenance and mineral potential integrates all previous government till surveys in the region.

The uplands south of Wager Bay coincide with a relatively stable position of the Keewatin Ice Divide (KID) and are dominated by a mixture of bouldery till blankets and veneers, weathered bedrock and diamictons, and boulder fields. The deeply weathered terrain under parts of the KID indicates the preservation of a pre-LGM landscape under cold-based ice conditions. South of the divide, the predominant regional trend of streamlined bedrock and till landforms varies from SSE to SE, parallel to main striation directions. A complex system of subglacial meltwater corridors and proglacial meltwater channels overprints the streamlined till that extends away from the KID. A later S to SSE deglacial event locally cross-cuts the streamlined terrain and corridors suggesting a northward ice margin retreat. The post-glacial marine limit increases from ~118 m asl southwest of Wager Bay near Paliak Islands to 140 m along Roes Welcome Sound and stays relatively constant at 140-150 m westward towards Tehery Lake.

A total of 73 regional till samples collected in 2015 and 2016 to evaluate mineral potential and characterize regional transport across the KID were analyzed for matrix texture, colour, carbon content, indicator minerals, pebble count, as well as geochemistry of the <0.063 mm fraction. All field observations (202 stations) and till composition datasets were compiled in separate spreadsheet files. Surface till consists of a silty sandy, granitic-rich diamicton and is commonly bouldery on the surface. Till has a significant local component and its composition reflects the underlying bedrock glacially transported away from the KID. The eastern sector is dominated by more immature tills, higher in sand content but with relatively high clay contents derived from highly erodible, poorly resistant weathered lithologies preserved under the KID. The distribution of heavy minerals picked as potential kimberlite indicator minerals (KIMs) in surface tills suggests glacial dispersal from diverse ultramafic and mafic bedrock sources: the Nanuq kimberlite field, mafic to ultramafic bodies within the Lorillard domain, undeformed ultrapotassic mafic intrusions, and possibly unknown kimberlite. In particular, the distribution of Ca-forsterite, eclogitic garnet and Cr-pyrope forms a 60-km long SSE-trending regional dispersal train from the Nanuq kimberlite bodies, parallel to the dominant ice flow direction. On the other hand, the presence of a significant number of Cr-pyrope, eclogitic garnet, Ca-forsterite, low Cr-diopside and bronzite grains in till south of Meen Lake suggests a clear potential for a local kimberlitic source up-ice (northwest) of the sample. The potential for Ni-Cu, platinum group elements (PGEs) and chromite mineralization in the region mainly lies in Archean komatiite/pyroxenite/peridotite ultramafic bodies of the Lorillard domain as shown by a large SE trending fan-shaped dispersal train of forsterite and a shorter SE dispersal train of chromite grains. Elevated to moderate concentrations of base and precious metals, metamorphosed or magmatic massive sulphide indicator minerals (MMSIMs) and gold grains in gossan-rich till and down-ice of supracrustal rocks within the northern part of the Lorillard domain indicates potential for base- and precious metal mineralization in this area. Smaller gossanous horizons were mapped in several other supracrustal panels (e.g. Pennington belt) north of the Chesterfield shear zone and till composition in this area indicates potential for metamorphosed volcanogenic massive sulphide (VMS) deposits.

## INTRODUCTION

The Geological Survey of Canada completed targeted surficial geology studies and glacial sediment sampling in 2015 and 2016 as part of the GEM-2 Tehery-Wager Activity of the Rae Project (Byatt et al., 2015, 2016, 2019a-b; Byatt, 2017; McMartin et al., 2015a-b, 2016a-c; Randour et al., 2016a-b, 2017a-b; Randour and McMartin, 2017; Randour, 2018). Concurrent bedrock (Wodicka et al., 2015, 2016a-b, 2017a-b; Steenkamp et al., 2015, 2016, 2017; Peterson et al., in prep) and gravity (Tschirhart et al., 2016) studies were also completed in the same area. The study area, which straddles parts of the Keewatin Ice Divide (KID), is covered by variable thicknesses of Quaternary sediments in an area of continuous permafrost, and lies south of the Ukkusiksalik National Park on the northwest side of Hudson Bay (Fig. 1). The main objective of the Tehery-Wager GEM-2 surficial geology component is to provide a glacial and post-glacial history framework required for interpreting the nature and provenance of surficial sediments. The work is a follow-up to GEM-1 reconnaissance scale bedrock mapping, till and stream sediment surveys in the Tehery-Cape Dobbs region in 2012 (Day et al., 2013; McMartin et al., 2013: Wodicka et al., in prep). This report presents an overview of the regional bedrock geology, summarizes the surficial geology and ice-flow chronology, and provides a detailed description of the field and analytical methods regarding the surficial geology component. The report also releases the complete field database and analytical results from the 2015 and 2016 till sampling surveys. A preliminary interpretation regarding till provenance across the Keewatin Ice Divide and implications for mineral potential in the region is presented.


*Figure 1. Location of study area in mainland Nunavut (red outline). Inuit owned lands are shown in orange. Field camps ran by the Geological Survey of Canada (GSC) and the Canada-Nunavut Geoscience Office (CNGO) in 2015 and 2016 are indicated by red stars.*

## Location and physiography

The study area is south of Wager Bay and east of Roes Welcome Sound in the northwest part of Hudson Bay, central mainland Nunavut, between latitudes 64° and 66° N and longitudes 87° and 93° W (Fig. 1). The area covers two complete 1:250 K NTS map sheets (56A, 56B) and parts of six others (46E, 46D, 56C, 56F, 56G, 56H) over approximately 44,000 km$^2$ (Fig. 2). It lies entirely within the Wager Bay plateau Ecoregion of Canada (http://ecozones.ca/english/region/30.html) and is underlain by Archean rocks of the Canadian Shield that form broad, sloping uplands, plains, and valleys. Elevations in the study area range from sea level rising gently westward and northwestward from Roes Welcome Sound and Chesterfield Inlet into uplands at 610 m asl along the National Park boundary in NTS 56G. Steep rocky hills rise abruptly from the southwest shores of Wager Bay into the uplands. Local relief is generally low, except for the southwestern shores of Wager Bay, and characterized by gently rolling hills and dissected upland plateaus, interspersed by wide valleys along the Lorillard, Borden and Gordon rivers, and flat coastal rocky lowlands along Roes Welcome Sound and Daly Bay. Drainage towards Hudson Bay is northward via the Wager Bay basin in the extreme north, and southward in the Lorillard River basin which is the dominant drainage way in the area (Fig. 2). A low arctic ecoclimate with a mean annual temperature of ~ -11°C (summer mean = 4.5°C; winter mean = -26.5°C) and mean annual precipitation between 200 and 300 mm characterizes the Wager Bay plateau. It is underlain by continuous permafrost with low ice content and a discontinuous cover of shrub tundra vegetation. Turbic and Static Cryosols are the dominant soils developed on surficial deposits. Areas of Regosolic Static Cryosols are associated with marine deposits along the coast of Roes Welcome Sound.

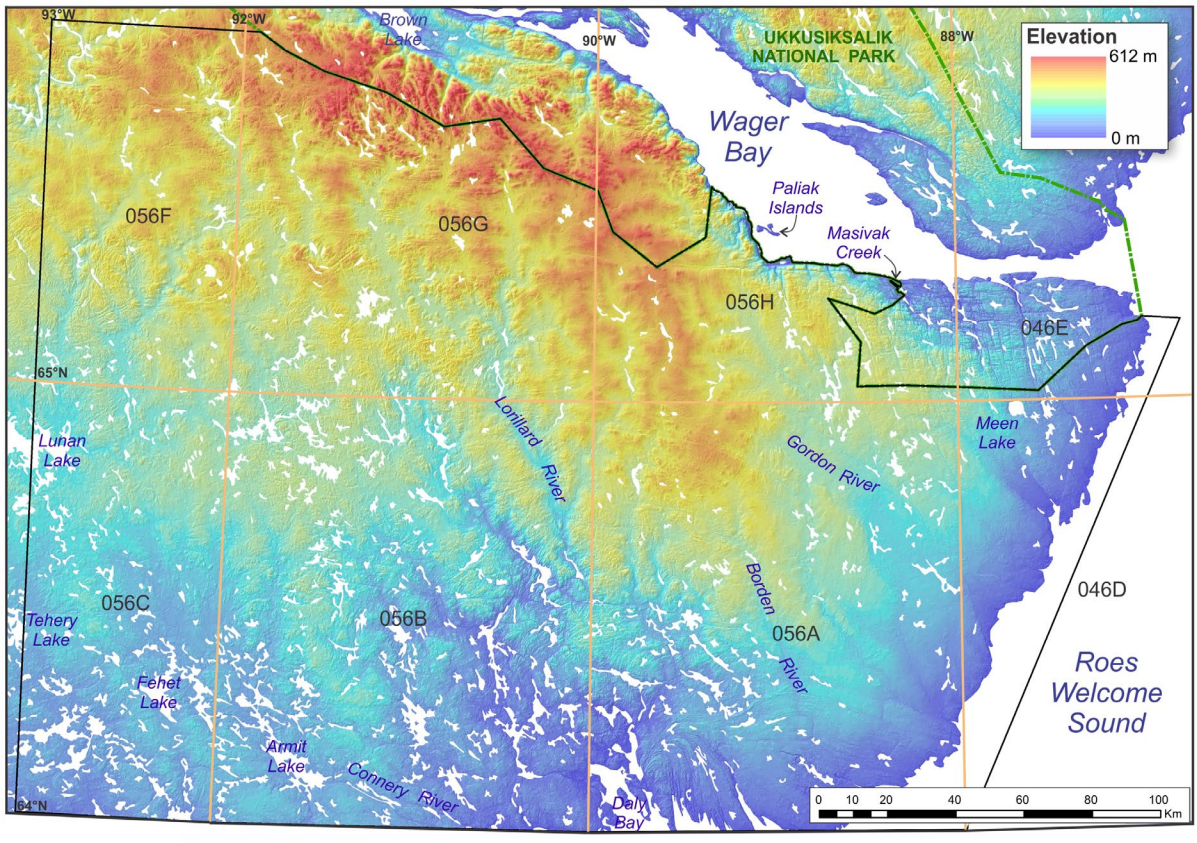


*Figure 2. DEM of the study area generated from CDED 1:50,000 topography. NTS maps sheets are labelled (e.g. 056G).*

**Bedrock geology**

The till sampling survey area lies within the south-central part of the Archean Rae craton of the Western Churchill Province, which represents a large mobile belt that formed during assembly of the supercontinent Nuna between ca. 1.98 and 1.80 Ga (e.g., Hoffman, 1990; Lewry and Collerson, 1990). The Rae craton mainly comprises Meso- to Neoarchean tonalitic to monzogranitic orthogneiss and volcano-sedimentary sequences, all of which are intruded by younger Neoarchean felsic plutons (e.g., Skulski et al., 2003; Corrigan et al., 2013; Hinchey et al., 2011; Pehrsson et al., 2013; Sanborn-Barrie et al., 2014). Paleoproterozoic supracrustal assemblages, now preserved in a number of structural basins, were subsequently deposited across the Rae craton (e.g., Rainbird et al., 2010).

The Tehery-Wager study area can be subdivided into six crustal domains (Fig. 3; Steenkamp et al., 2015, 2016, 2017; Wodicka et al., 2015, 2016a, 2017a,b, and references therein; Peterson et al., in prep.). The central, north-south oriented supracrustal-rich domain (Lorillard domain) comprises the ca. 2.70 Ga Lorillard supracrustal belt and intercalated ca. 2.90-2.67 Ga gneissic and plutonic rocks. The upper amphibolite-facies Lorillard supracrustal belt consists of quartzite, semipelite, garnetite, silicate-facies iron formation, amphibolite, metagabbro, peridotite, calc-silicate, and rare marble. Anomalous concentrations of Ag, Cu, Bi, Au, and Co-Fe arsenide minerals in till and/or stream sediments within and adjacent to this belt highlight the belt's potential to host base- and precious-metal mineralization (Day et al., 2013; McMartin et al., 2013).

The Lorillard domain separates two dominantly Archean tonalitic to granitic domains, the ca. 2.71-2.66 Ga Lunan domain to the west and the ca. 2.86-2.70 Ga Gordon domain to the east, which are characterized by contrasting populations of Nd model ages (Wodicka et al., 2017a,b; Peterson et al., in prep.). The Paleoproterozoic granulite-facies Daly Bay complex in the southeastern part of the study area is dominated by 1.92-1.91 Ga tonalite-monzogranite and anorthosite-gabbro (Gordon, 1988; Hanmer and Williams, 2001; Wodicka et al., in prep.). Paleoproterozoic supracrustal rocks (Kingmirit belt) in a fault-bounded panel in the immediate footwall to the Daly Bay complex contain several gossanous horizons and are cut by numerous granitic veins with sparse tourmaline, fluorite, and scheelite, suggestive of greisen-style tungsten mineralization (Garrison, 2016).

To the southwest, the granulite-facies Kummel Lake domain, dominated by ca. 2.71-2.65 Ga monzogranite-granodiorite and anorthosite-gabbro, and supracrustal rocks of unknown age, may be related to the Uvauk complex (Mills et al., 2007) south of the map area. The complexly folded Chesterfield shear zone separates the Lunan, Lorillard, and Gordon domains from the Douglas Harbour domain to the north. The latter domain, transected by the Paleoproterozoic dextral transcurrent Wager shear zone, consists largely of 2.71-2.69 Ga tonalitic-granitic rocks and supracrustal rocks of the Archean Paliak and Paleoproterozoic Pennington belts. The lower amphibolite-facies Pennington supracrustal belt, comprising thick quartzite interlayered with psammite, semipelite, pelite, and mafic rocks of probable volcanic origin, is thought to be correlative with the Ketyet River Group (e.g., Rainbird et al., 2010) exposed to the west of the map area. The belt contains several, m- to km-long gossanous horizons of unknown potential within altered semipelite and mafic rocks. The Paliak belt contains more diverse and distinct lithologies, including garnetite, iron formation, strongly migmatitic psammitic to semipelitic gneiss, ultramafic boudins, and mafic rocks, that bear many similarities with supracrustal rocks of the Lorillard belt. Diamond-bearing kimberlite within the Nanuq property, formerly held by Peregrine Diamonds Ltd., occur within the

Paleoproterozoic (1.83 Ga) Wager pluton and Ford Lake batholith that are intrusive into Archean basement of the Douglas Harbour domain (Fig. 3; white diamonds; Pell and Strickland, 2004).

With the possible exception of the Kummel Lake domain and Daly Bay complex, all domains of the Tehery-Wager region contain intrusions of ca. 2.62-2.58 Ga gabbro through granite of the Snow Island suite (Peterson et al., 2015), and ca. 1.84-1.82 Ga dykes, sills or large intrusions of the Hudson granite suite (van Breemen et al., 2005). Rapakivi monzogranite of the Snow Island suite Borden complex (Fig. 3) and nearby Hudson monzogranite contain molybdenite grains and elevated concentrations of Pb, Mo, and/or Sn, which could be related to intrusion-hosted polymetallic mineralization (Wodicka et al., 2016b, 2017a). Intrusions of coarse, ca. 1.83 Ga mafic plutonic rocks and syenite, present only in the Lorillard, Lunan, and Douglas Harbour domains, are interpreted to represent the intrusive equivalents of potassic to ultrapotassic, mafic to syenitic dykes of the ca. 1.83 Ga Dubawnt minette (Peterson et al., 2002). Late, northwest-trending diabase dykes, thought to belong to the ca. 1.27 Ga Mackenzie dyke swarm (LeCheminant and Heaman, 1989), cut all rock types and structural elements, with the exception of younger brittle faults.

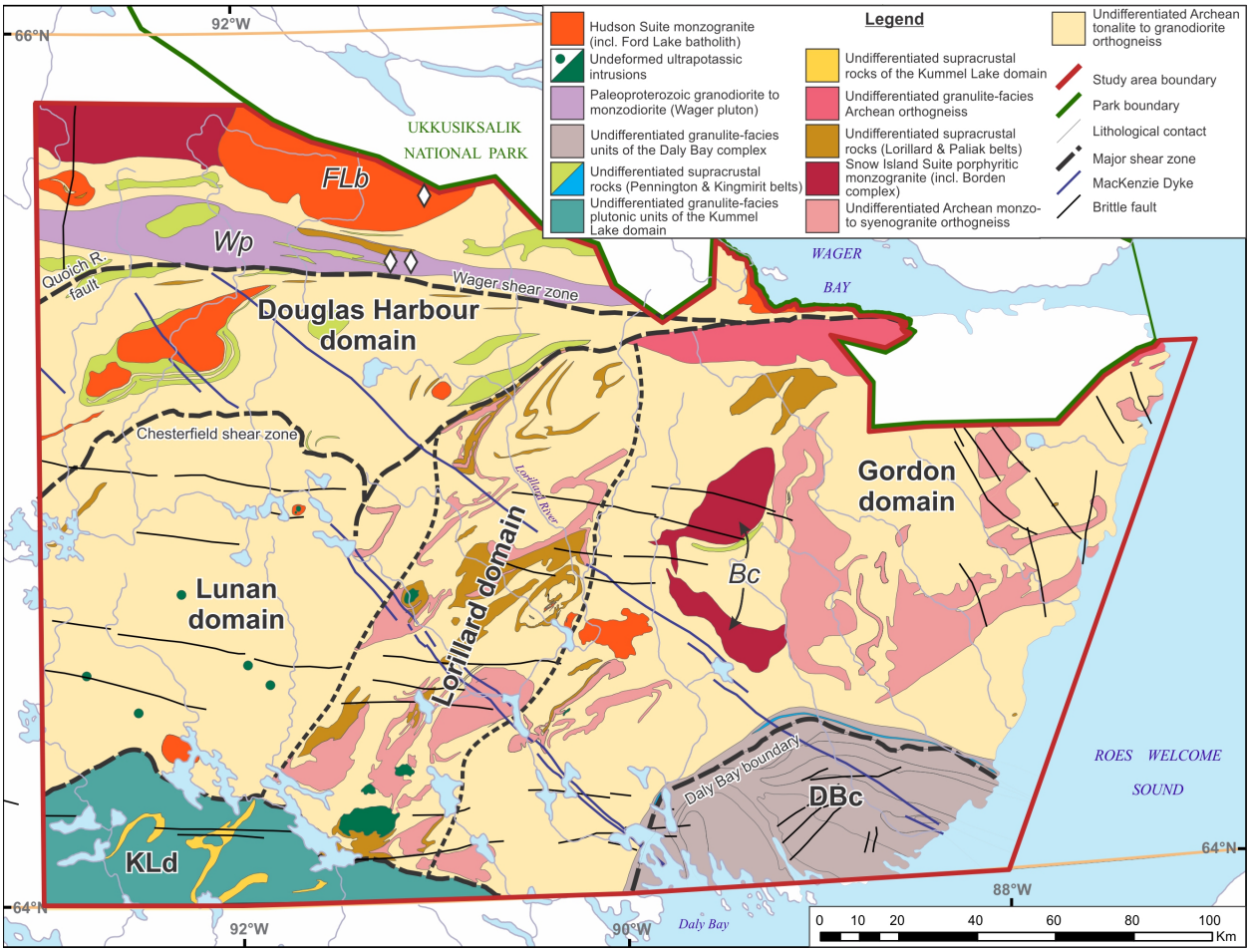


*Figure 3. Simplified geological map of the Tehery-Wager area with interpreted geological domains (modified from Steenkamp et al., 2015 and Wodicka et al., 2016a, 2017a). White diamonds indicate known kimberlite localities originally discovered by Peregrine Diamonds Ltd. and joint partners. Abbreviations: Bc = Borden complex; DBc = Daly Bay complex; FLb = Ford Lake batholith; KLd = Kummel Lake domain; Wp = Wager pluton.*

## Quaternary Geology

*Regional context and previous work*

The Tehery-Wager area was covered by Keewatin Sector ice of the Laurentide Ice Sheet during the last glaciation (Late Wisconsin) (e.g. Dyke and Prest, 1987) and located under the northeastern end of a major ice divide zone (Keewatin Ice Divide: Lee et al., 1957) from which ice flowed in opposite directions (Fig. 4). Streamlined landforms and scattered striations indicate a regional glacial flow direction to the southeast over most of the area except in the northwest part where ice-flow indicators trend in an opposite direction, to the northwest (i.e. Prest et al., 1968; Aylsworth and Shilts, 1989). South-southeastward esker systems commonly cross-cut the southeast direction of the streamlined landforms south of the ice divide.

The western part of the project area (NTS 56B-C-F) was mapped for surficial geology at a reconnaissance scale with little or no ground truthing (Aylsworth, 1990a, b; Thomas and Dyke, 1981). Landforms on these maps showed an uncertain direction for the former ice flow: entirely northward in the Pennington Lake map sheet (NTS 56F: Thomas and Dyke, 1981) and southward in the Tehery Lake map sheet directly south (NTS 56C: Aylsworth, 1990a). More systematic, field-based surficial geology mapping by Dredge and McMartin (2007) in NTS 56G suggested the KID was stable for a long time in the uplands southwest of Wager Bay and coincided with the presence of a weathered landscape potentially preserved under cold basal ice conditions (McMartin and Dredge, 2005). Regional till composition indicated a local provenance, extensive subglacial and pro-glacial meltwater reworking of glacial sediments, and poorly defined glacial dispersal trains (Dredge et al., 2005, 2006). The post-glacial marine limit was mapped to an elevation of 110 m in the inner part of Wager Bay, decreasing westward to about 95 m west of Brown Lake (Dredge and McMartin, 2005). More recently, preliminary surficial geology maps were compiled in the southeastern part of the study area during the GEM-1 program (Dredge et al., 2013a-c: NTS 46D and 56A). Major subglacial meltwater corridors trending SE, cross-cut by SSE-trending eskers, and glacial sediments variously reworked by glacial meltwater and/or marine action, suggest a complex deglacial history that can affect the interpretation of till composition for mineral exploration.

Quaternary geology studies, surficial mapping and till sampling were completed in regions adjacent to the study area. Smith's (1990) work in the National Park brought to light a complex late glacial history for the immediate areas surrounding Wager Bay. Much of this work was based on the interpretation of glacial geomorphology, in particular till landforms and meltwater channels. South of Wager Bay within the Park's boundary, glacial landforms were interpreted as indicating mainly southeast flowing ice, following an early phase to the south. In the northwest part of the park, paleo-flow towards the north-northwest was interpreted from glacial flutings from an ice divide lying south of Wager Bay and continuing east across the bay in the Paliak Islands area (see location on Fig. 2). Glacial retreat was thought by Smith to be entirely northward within the Park's area and not towards the last position of the ice divide south of Wager Bay. North of Wager Bay, McMartin et al. (2015c) mapped and characterized glacial transport within a large ice stream flowing north towards Committee Bay from the Keewatin Ice Divide. These authors also recognized major ice-flow reversals into Wager Bay as a result of drawdown into the opening marine waters during the latest deglaciation phases. Drift lineations (including some superimposed with cross-cutting relationships), potential areas of cold-based ice, ice-streaming landscapes and end moraines were mapped at regional scale based on remotely sensed data such as satellite imageries and digital elevation models (Boulton and Clark, 1990; Clark, 1997; De Angelis, 2007; De Angelis and Kleman, 2005, 2007, 2008; Kleman et al., 2002, 2010; Margold et al., 2015, 2018). The lack of ground truthing and detailed mapping in these studies prevented a comprehensive understanding of the glacial history.

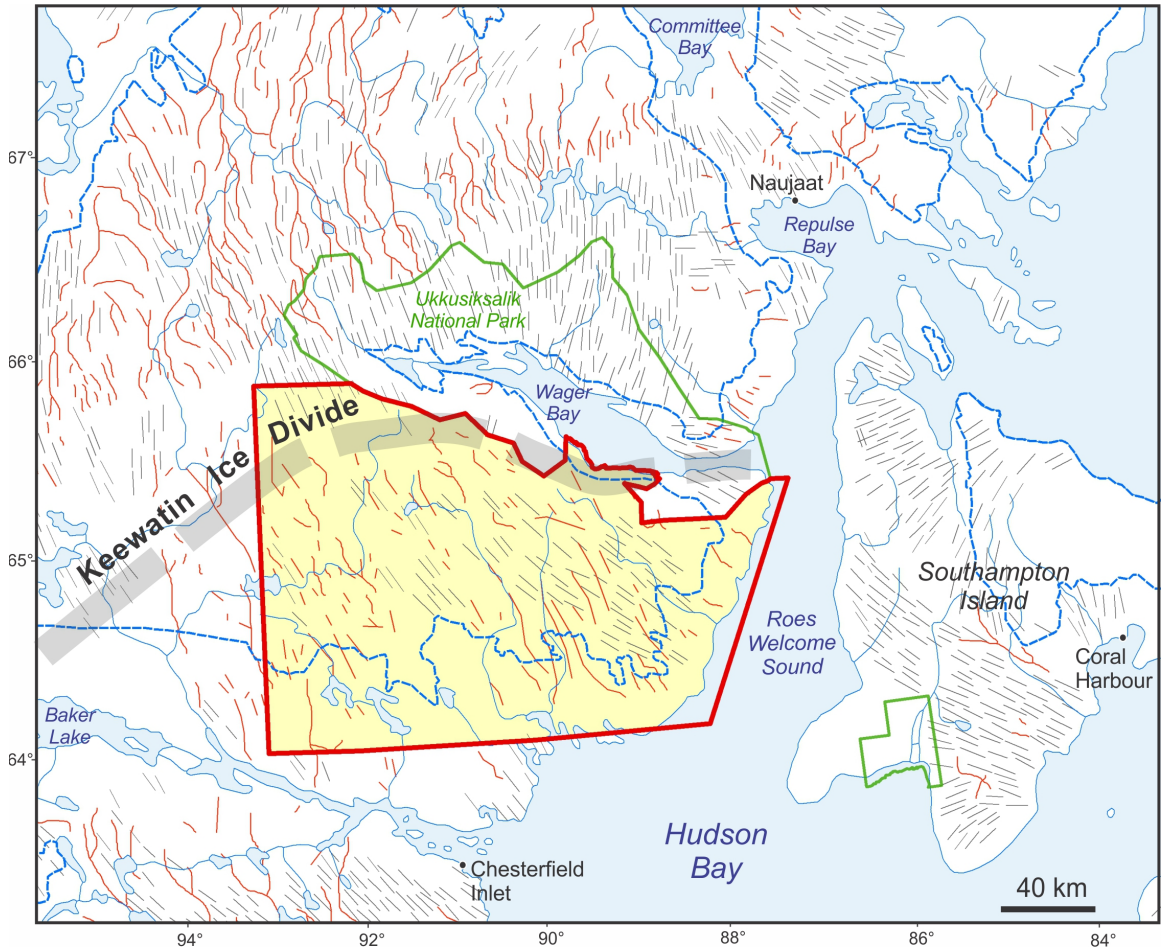


*Figure 4. Regional map showing location of eskers (red lines), streamlined landforms (grey lines) and marine limit (dashed blue line) derived from Prest et al. (1969). Axis of KID is from McMartin et al. (2016b, 2017). Tehery-Wager GEM2 study area is outlined in red.*

*Summary of the surficial geology and ice-flow chronology*

Tills and glacial diamictons of different nature, thickness and provenance form the predominant surficial geology units in the study area (Fig. 5). Targeted surficial geology mapping indicates that the uplands south of Wager Bay and Brown Lake that coincide with the KID zone are dominated by a mixture of till blankets and veneers, weathered bedrock and diamictons, boulder fields and felsenmeer (McMartin et al., 2015a,b, 2016a-c). The deeply weathered terrain forms an extensive area 50 km by 15 km southwest of Wager Bay mainly above 400 m a.s.l. (Fig. 6; Fig. 7a,b). West of the weathered terrain, the ice divide zone is characterized by thick bouldery till, including areas with giant ice-wedge polygons (Fig. 7c), or widespread boulder fields and thin bouldery till with few lakes and rare outcrops (Fig. 7d). The high proportion of boulders in till over and directly down-ice of the KID may be an indication of its immaturity and short glacial transport (Fig. 8a). On either side of the KID zone, a swath of streamlined, thin and thick silty sand till extends outward to the southeast and northwest (Fig. 8b). South of the ice divide, a complex system of subglacial meltwater corridors and proglacial meltwater channels have eroded the various till units (See Fig. 5). The south-southeast to southeast-trending corridors vary in width from 0.5 to 4 km and start immediately south of the KID central axis; they comprise large eskers, pitted outwash plains, small irregular hummocks and ridges, short streamlined and blunted subglacial landforms, eroded till remnants, boulder lags, and washed bedrock surfaces (Fig. 9a,b). Continuous south- to south-southeast-trending

eskers cross-cut some of the corridors and streamlined till in the central and eastern part of the area suggesting that ice flow close to final deglaciation was different from that prior to deglaciation, and that the ice margin was reoriented during northward retreat to the uplands. Where proglacial meltwater channelized systems abound, especially in NTS 56G and 56H, till surfaces show extensive erosion and/or reworking, leaving erosional remnants of reworked till, boulder lags, boulder pavements and washed bedrock surfaces, with bouldery alluvial bars and sandy outwash fans and terraces at their distal ends (Fig. 10a, b). Nested lateral meltwater channels are confined in areas close to the final remnants of the KID indicating cold-based deglaciation in the uplands. Extensive areas of bedrock outcrops extend far inland along the coast between Chesterfield Inlet and the outer part of Wager Bay. Folds and faults as well as small glacially scoured basins occupied by a myriad of shallow lakes are prominent features of the bedrock topography in these areas.

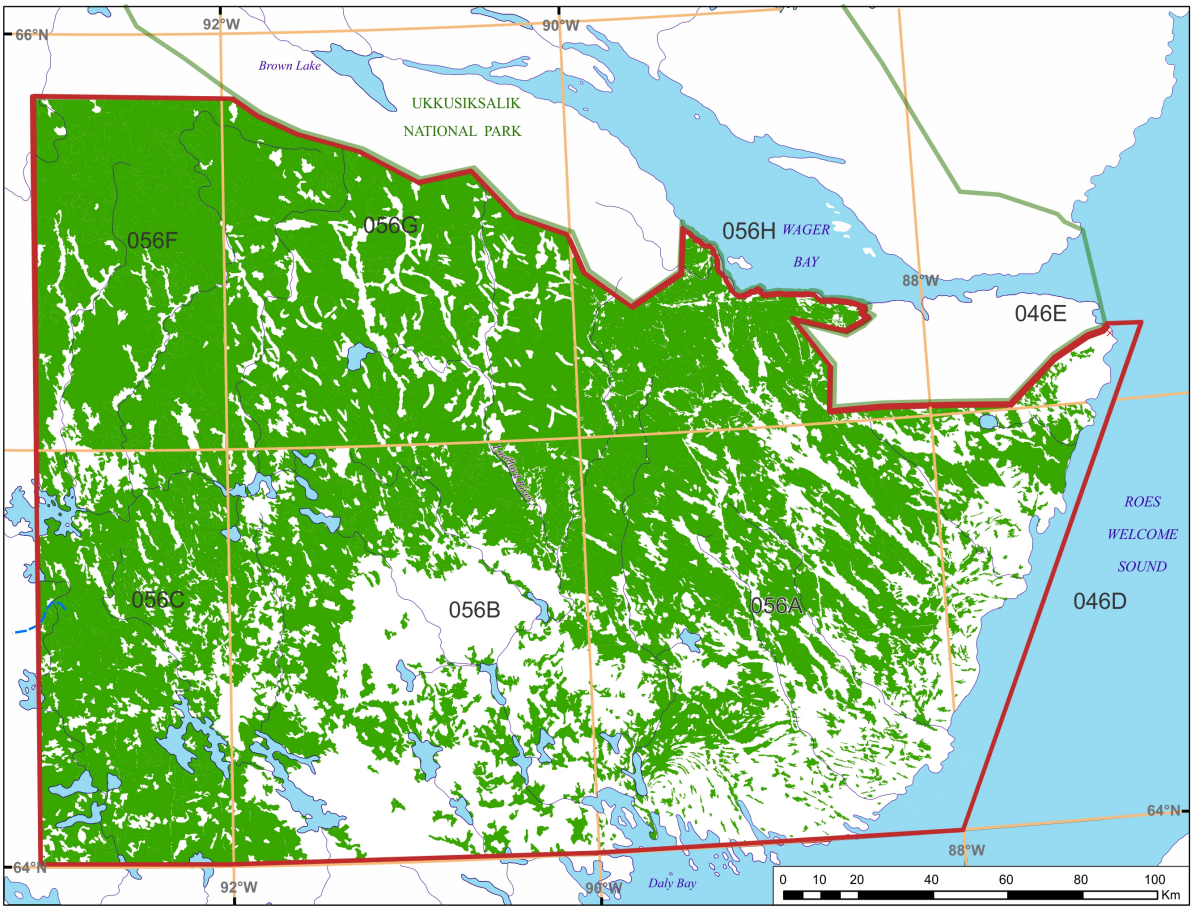


*Figure 5. Till units of various nature cover over 75% of the study area. Undifferentiated till units shown in green are derived from surficial geology maps (Thomas and Dyke, 1981; Aylsworth, 1990a, b; Dredge and McMartin, 2007; Randour and McMartin, 2017; Randour et al., in press).*

Ice flow indicators in the study area indicate a complex history but can be regrouped into three main sets: 1) the ice flow sets over the ice divide zone, 2) those oriented south (S, SSE, SE, ESE) south of the KID, and 3) those oriented north (NNW and NNE) north of the KID (Fig. 6).

1) The ice divide zone itself is relatively narrow and characterized by either the absence of ice-flow indicators (i.e. weathered terrain or block fields) or opposing indicators on a single outcrop (i.e. NNW vs SSE). Along the southern shores of Wager Bay, early N and NNE ice flows, as well as late ice flows into (NE) and parallel (ESE) to the bay, are observed in the landform and striation record and suggest the KID was located along and inland south of the bay. The early northward directions are not observed at Masivak

Creek and further east within NTS 46E, where the dominant ice flow directions revert to the SE, hence confining a narrow zone where the central axis of the KID continued into Wager Bay. Further west in NTS 56F, a zone without ice flow indicators, and opposing trends on either side, is found around latitude 65°30', indicating the location of the ice divide axis in the middle of the map sheet rather than at the boundary between 56F and 56C. Together these ice flow patterns indicate the KID was a relatively stable feature in the uplands south of Wager Bay during most of the last glaciation and deglaciation, and did not migrate more than 20 km, in contrast to the extension of the KID near Baker Lake (e.g. McMartin and Henderson, 2004).

2) South of the KID, the predominant regional trend of streamlined till features and striations indicates ice flow varying between SSE and SE, parallel to major 1st generation eskers and meltwater corridors. An earlier event to the south is indicated by old striations and large-scale streamlined bedrock landforms. The later more SSE-trending eskers, parallel to late SSE striations, cross-cuts the southeast streamlined terrain and subglacial meltwater corridors, and represent recessional features that formed after Daly Bay and Roes Welcome Sound were ice-free; they indicate a NNW retreat as the ice disappeared towards the ice divide's final remnants. In patchy areas along and west of Lorillard River, as well as towards the uplands of Wager Bay, the dominant streamlined landforms, eskers and striations are all aligned to the SSE, unlike the palimpsest landscape described above.

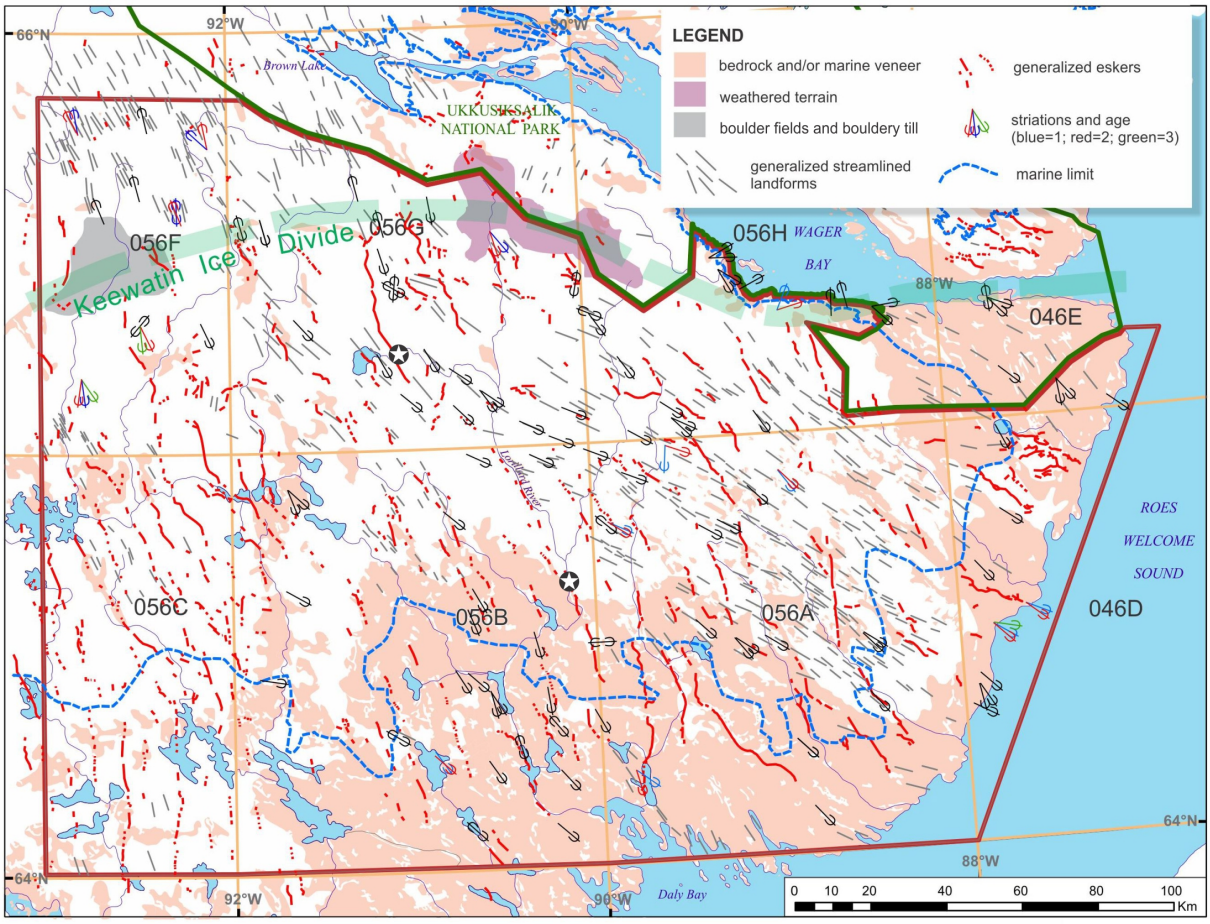


*Figure 6. Generalized landform and striation map (from McMartin et al., 2016b). Striations from GEM-1 and GEM-2 field work; eskers and bedrock areas from Aylsworth and Shilts (1989); marine limit from Dredge and McMartin (2005) in NTS 56G, McMartin et al. (2015c) north of Wager Bay and Randour et al. (2016b) in the rest of the area. White areas include mainly undifferentiated till and glaciofluvial units. Field camps are indicated by stars.*

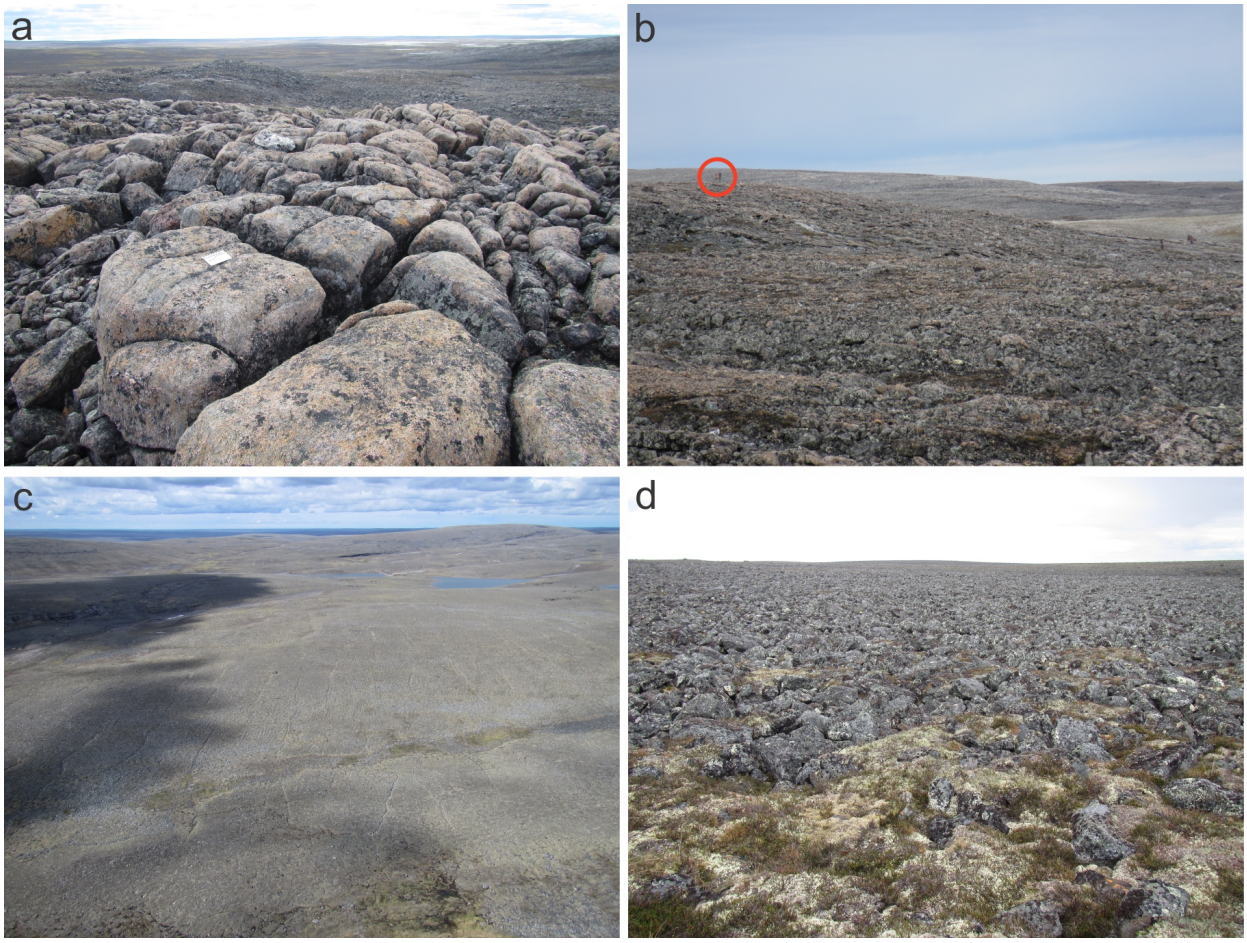


*Figure 7. Photographs of various glacial landscapes under the Keewatin Ice Divide: a) deeply weathered Hudson granite outcrop (16MOB144; scale is 8 cm long); b) weathered bedrock and diamictons in upland plateau (near 16MOB144; caribou as a scale); c) thick bouldery till with giant ice-wedge polygons – 200 x 200 m (near 16MOB154);d) boulder fields with few lakes and rare outcrops (16MOB165).*

3) North of the KID in NTS 56F and 56G, streamlined landforms and striations indicate a predominant NNW ice flow direction. Outside the study area in the National Park, a later NNE flow is indicated by streamlined landforms just down-ice of the weathered terrain (i.e. Dredge and McMartin, 2007).

Detailed mapping and elevation measurements of the marine limit as part of an MSc research project (Randour et al., 2016a-b, 2017a-b; Randour and McMartin, 2017; Randour, 2018) show significant spatial variation, increasing eastward from about 95 m around Brown Lake to 140 m near Roes Welcome Sound, in contrast to the westward increase shown on the Glacial Map of Canada (Prest et al., 1968). The marine limit remains relatively constant southward along Roes Welcome Sound and westward further inland, at elevations ranging between 140 and 150 m. Bouldery beaches, wave-washed bedrock surfaces, terraces, glaciomarine deltas and wave-cut notches in till are found along the marine limit. Erosive features are mostly found on steep slopes south of Wager Bay while depositional features are predominant in flat-lying terrains, such as those along Roes Welcome Sound and Daly Bay. Below the marine limit, lowlands that skirt the coasts of Roes Welcome Sound and Chesterfield Inlet show evidence for post-glacial marine erosion and reworking of thin glacial and glaciofluvial sediments; marine veneers are silty sandy and occur as scattered deposits between bedrock ridges or glacial landforms; thicker marine sands and silts are limited

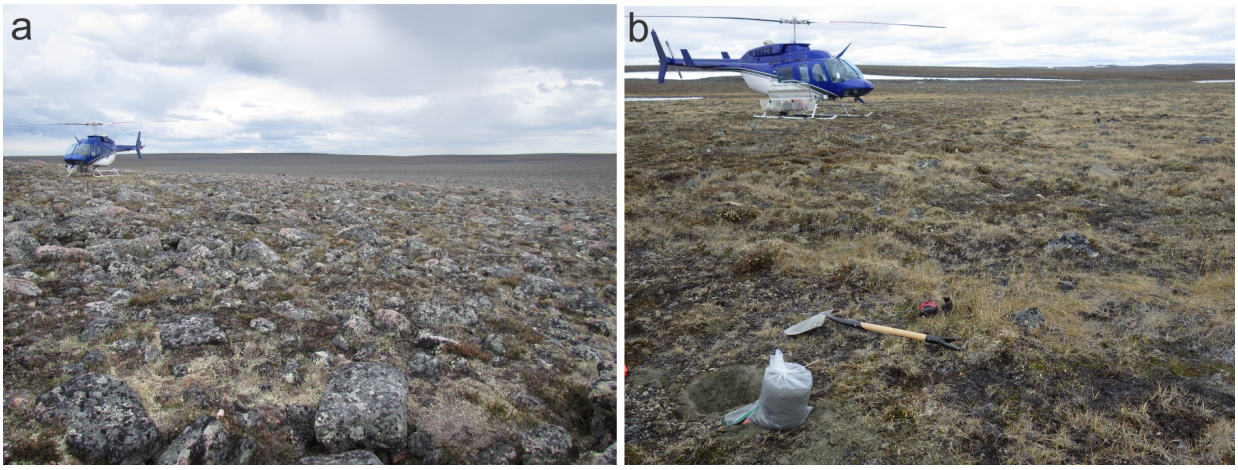


*Figure 8. Photographs of two contrasting till types: a) bouldery, immature sandy till north of KID near National Park's boundary (16MOB156); b) thick, silty sand till in streamlined landform in NTS 56G (15MOB058).*

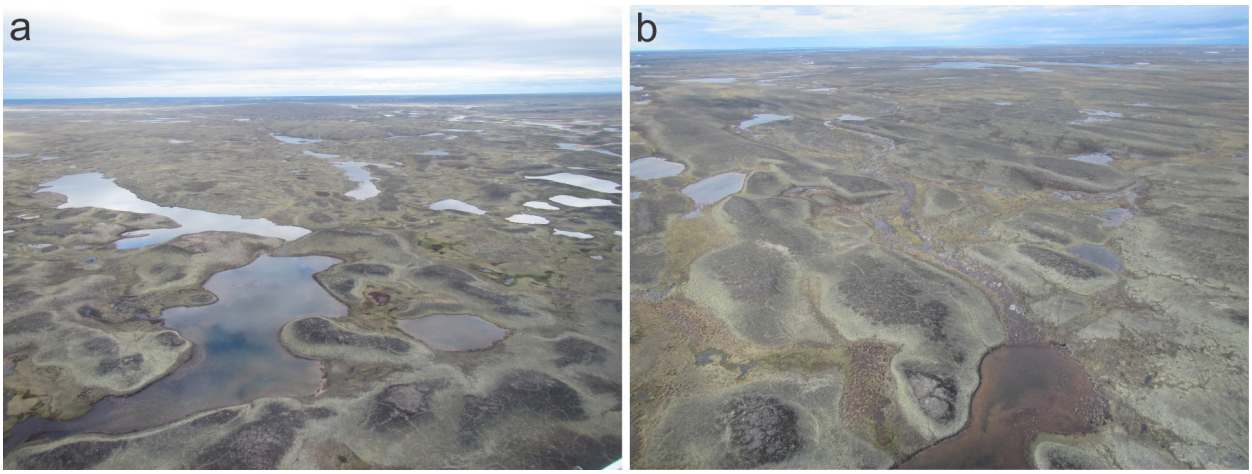


*Figure 9. Photographs of various landforms in subglacial meltwater corridors SE of KID: a) hummocks and small ridges; b) streamlined and blunted subglacial landforms.*

and only found along narrow major river embayments, or adjacent to a few large eskers within the meltwater corridors that extend to the coast.

A surficial earth materials mapping MSc research project using advanced remote predictive mapping (RPM) methods produced surficial materials classification maps validated with georeferenced sites for areas south and north of Wager Bay to support surficial geological mapping efforts in the region (Byatt et al., 2015, 2016; Byatt, 2017; Byatt et al., 2019a-b). For an area south of Wager Bay (NTS 46D, 46E, 56A, 56H), a map with 22 surface material classes was produced using a non-parametric classifier, Random Forests, applied to a combination of RADARSAT-2 C-band dual- polarized (horizontal transmitted and horizontal received (HH) and horizontal transmitted and vertical received (HV)) and Landsat-8 OLI images with a digital elevation model and slope data (Byatt et al., 2019b). The results show that the addition of RADARSAT-2 C-HH and C-HV images to the optical Landsat-8 OLI image in the classification process increases the overall classification accuracy from 96.7% to 99.3%. The resulting map was compared to 648 georeferenced sites with field observations or interpreted from aerial photographs/Google Earth to determine the mapping accuracy. Similarly, the mapping accuracy increases from 72.1% to 78.0% when adding RADARSAT-2 images. The material classes with the highest mapping

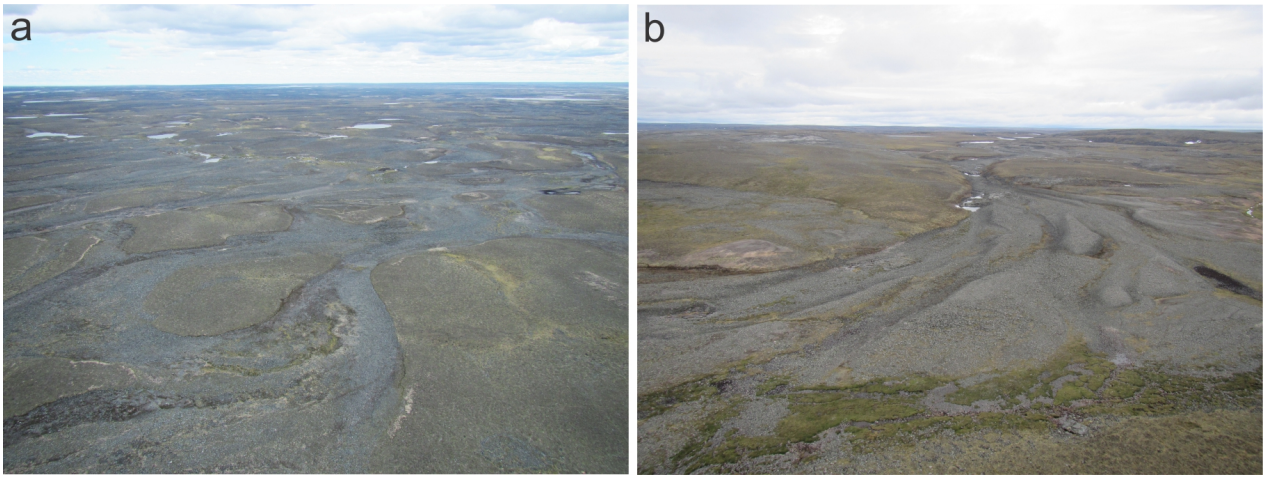


*Figure 10. Photographs of proglacial meltwater channelized systems in NTS 56G south of the ice divide: a) erosional remnants of reworked till; b) bouldery alluvial bars at distal end of proglacial channel.*

accuracies were *flooded alluvium* and *boulders*, both with 100%. The class with the lowest mapping accuracy was *thin sand and gravel over bedrock* (11.1%), commonly confused with *sand and gravel with vegetation* and *bedrock*.

## FIELD METHODS

### Field data collection

Surficial geology observations were collected in July 2015 and July 2016 at sites mainly accessed by helicopter or along short foot traverses from GSC-CNGO camps on Lorillard River (Fig. 11). The work involved collecting observations on surface sediments, glacial landforms, periglacial features and small-scale ice-flow indicators on bedrock, measuring the elevation of the post-glacial marine limit (see detailed methods in Randour et al., 2016b), ground truthing of preliminary remote predictive maps (see Byatt et al., 2015, 2019b), till sampling, and sampling age dating materials. Sites and traverses were chosen based on previous work, nature of the surficial geology as observed on air photos, satellite imagery and DEM, targeted bedrock units and/or geochemical anomalies, and logistics shared with other project participants (see Wodicka et al., 2015, 2016a). A total of 202 sites were visited and are described in Appendix 1. The orientation and sense of 110 small-scale glacial erosional features on bedrock were measured at 80 sites (see Fig. 6). Relative ages of striated facets were established at 14 sites. Ice-flow indicator measurement locations and descriptions are provided in Appendix 2.

### Till sampling

In 2015, 33 regional till samples were collected to provide more detail on geochemical anomalies identified in 2012, or to support bedrock mapping in areas covered by thick drift (Fig. 11). Some of these samples were also collected at approximately 10-km intervals along a 140-km long transect parallel to ice-flow (SE) to characterize the regional glacial transport (T1); the transect overlaps parts of a regional Mg-rich olivine SE-trending dispersal train in till (McMartin et al., 2013) and crosses the NE-SW trending Lorillard supracrustal belt that showed anomalous concentrations of Ag, Cu, Bi, Au and Co-Fe arsenide minerals in till and/or stream sediment samples (Day et al., 2013; McMartin et al., 2013). In 2016, regional till samples were collected at 40 sites to provide more detail on geochemical anomalies identified in 2015,

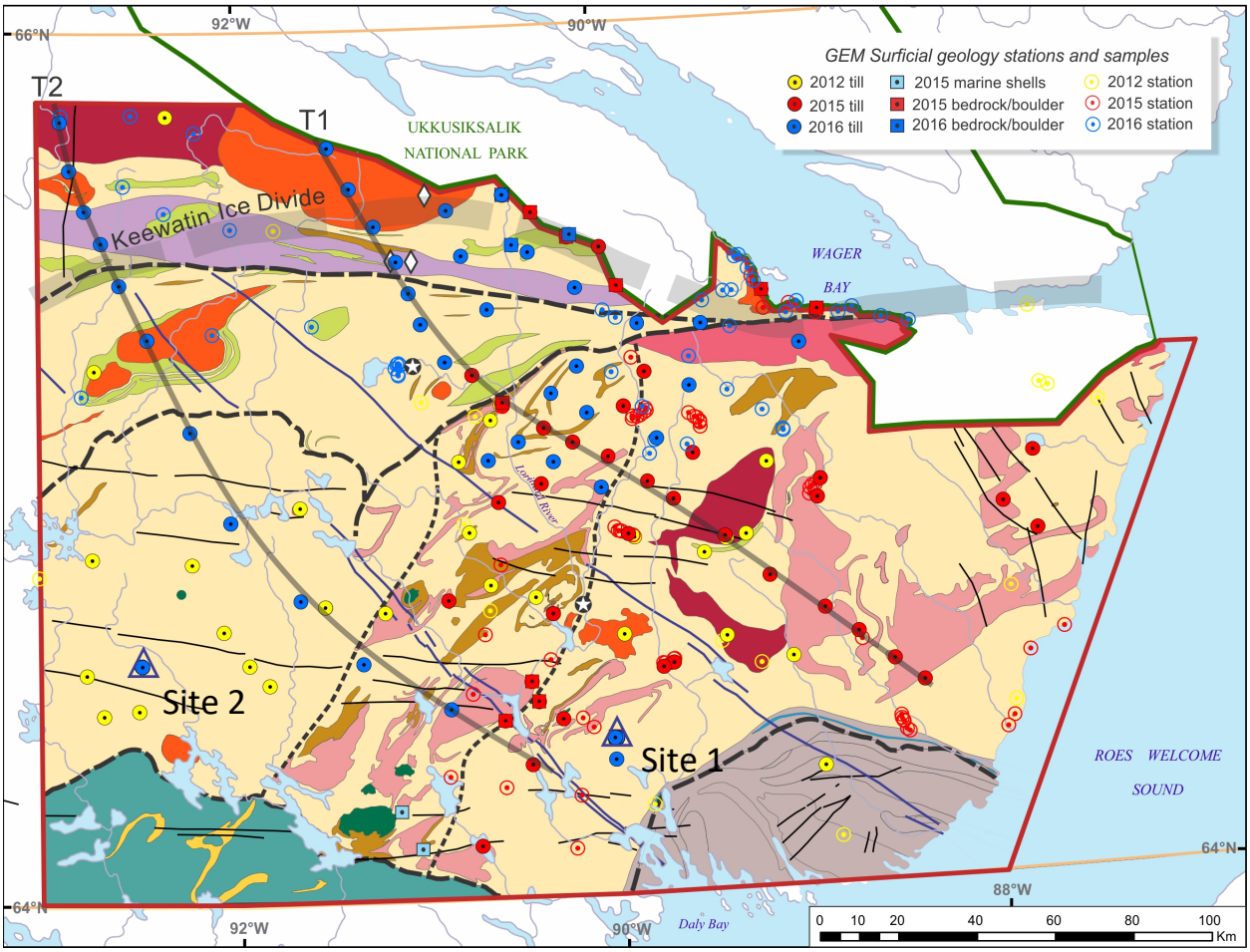


*Figure 11. Location map of till samples and surficial geology observations collected in 2012, 2015 and 2016 as part of GEM-1 and GEM-2 projects. T1 and T2 transects are indicated (see text). Bedrock and boulder samples collected for cosmogenic nuclide exposure dating are also shown, as well as the two marine shell samples dated for $^{14}C$. The two detailed sites sampled in 2016 for the marine reworking study are indicated with a triangle (see text). Bedrock legend is given in Figure 3. GSC-CNGO field camps are indicated by white stars.*

namely a chromite grain anomaly in the northern part of the Lorillard domain (Fig. 11). Till samples were also collected at about 10-25 km intervals along two transects roughly parallel to ice-flow and across the KID (T1-continued from 2015, and T2). T1 extends NW of the Lorillard supracrustal belt, intersects a SSE-trending kimberlite indicator mineral train derived from one of the Nanuq kimberlite pipes (Pell, 2008) as well as slivers of the Pennington and Paliak supracrustal belts, and encompasses the north side of the ice divide. The western transect (T2) also extends over the ice divide zone and crosses the Wager and Chesterfield shear zones, and the limit of post-glacial marine inundation. Regional till samples were carefully collected on flat till surfaces in Cy-horizon material from hand dug pits in frost boils, at an average depth of 35 cm. At each site, one small sample (~3 kg) and one large sample (mean=12.1 kg; range=9.3-15.1 kg) were collected in plastic bags. Field duplicate samples at about 5 m away from the original were collected at two of the regional sites.

In addition to the regional till samples, two selected sites at the marine limit were sampled in detail in 2016 to evaluate the effects of marine reworking on till texture and geochemical composition (see Fig. 11 for location; Randour et al., 2016b, 2017b; Randour, 2018). The first site is characterized by intensely wave-washed surfaces surrounded by bouldery beaches forming a distinct trimline with unmodified till-

covered surfaces above; the second site forms a clear trimline around a small topographic high forming wave-cut notches between intact till above and reworked till below the marine limit. At each site, two vertical profiles in till were sampled at approximately 10 cm intervals in frost boils down to the permafrost table: one located immediately above the marine limit and one located directly below. In addition to the profile samples, five field duplicate samples at an average depth of 40 cm were collected nearby each frost boil to measure site variability. A total of 54 small (~3 kg) samples were collected for this detailed study. Till sample locations and descriptions are provided in Appendix 3.

**Geochronological sampling**

Various materials were collected to help determine the relative age of the weathered bedrock terrain under the ice divide, to constrain the ice-margin retreat history or define the timing of the maximum post-glacial marine inundation (Fig. 11). Three different types of landscapes were sampled for terrestrial cosmogenic nuclide (TCN) dating.

1) Five bedrock samples were collected in weathered upland terrain southwest of Wager Bay under the Keewatin Ice Divide to determine the degree of inheritance and to constrain the relative age of potentially preserved (older) surfaces under a cold-based dome. The sampled outcrops consisted of highly weathered Hudson Suite granite or granitic gneiss (15MOB035, 15MOB053, 15MOB054, 15MOB055, 16MOB144) characterized by altered and open joint surfaces, ice-wedge polygons developed in thick weathered felsenmeer and grus, and the absence of glacially polished surfaces or ice flow indicators, except for a few glacially transported erratics. In this respect, one glacially transported sub-angular Hudson Suite granite boulder (16MOB147) resting on weathered and spalled granitic gneiss outcrop over the ice divide zone was sampled in 2016. This site was first visited in 2004 (McMartin and Dredge, 2005) and the weathered outcrop was sampled in 2015 (15MOB053); the age of the glacial erratic will be compared with the relative exposure age from the nearby weathered bedrock surfaces.

2) Three samples were collected to help determine minimum deglaciation ages. Directly above the marine limit west of the 2015 field camp, a glacially polished bedrock surface (15MOB109) and a sub-angular boulder perched (15MOB110) on smaller boulders were sampled. Another bedrock sample was collected from a glacially polished quartzite outcrop (16MOB146) within the Pennington supracrustal belt about 15 km from a weathered sample collected under the KID (16MOB144) to date the timing of deglaciation and compare relative erosion rates between glacially eroded and weathered bedrock surfaces.

3) Five bedrock samples were collected at or slightly below the post-glacial marine limit to date the timing of marine emergence (15MOB068, 15MOB069, 15MOB070, 15MOB074, 15MOB078). These sites are characterized by intensely wave-washed surfaces surrounded by bouldery beaches forming a distinct trimline with unmodified till-covered surfaces above. The exposure ages will help constrain the time of the maximum marine stand in Wager Bay and Chesterfield Inlet.

All sample sites for TCN dating were from non-vegetated flat outcrops (0°-4° slope) as far as possible from nearby slopes, or from the flat-top portion of the perched boulders to ensure that the surfaces had full exposure to cosmic rays (minimum shielding) after deglaciation or marine emergence. A ~25 cm x 25 cm grid surface was sawn on the outcrops/boulders and the ~2 cm thick cuttings (~2 kg) were removed

with a chisel. The lithologies collected were granitic in composition to ensure enough quartz mineral grains for $^{10}$Be and/or $^{26}$Al exposure age dating (Gosse and Phillips, 2001). Selected samples were analysed at the Cosmogenic Isotopic Science laboratory at Dalhousie University and the results will be reported and discussed elsewhere. Samples collected at the marine limit were analysed at Lamont-Doherty Earth Observatory of Columbia University. Preliminary $^{10}$Be ages obtained on these samples indicate that the marine incursion possibly occurred 500-1000 years earlier than depicted in $^{14}$C-based reconstructions (e.g. Dyke, 2004). Given the geological context, the $^{10}$Be ages also constrain the onset of deglaciation towards the continental interior, near the core of the Keewatin Ice Divide (Randour, 2018; Randour et al., in prep-1).

Marine mollusks are rare in the study area. Prior to this study, only one radiocarbon date from a site at 126 m elevation east of Borden River in NTS 56A was available for the entire region between Chesterfield Inlet and Wager Bay (GSC-289, Craig, 1965; corrected age of 6600±170 $^{14}$C yrs BP: 7108-7791 cal yrs BP). Marine shells were found at two sites in 2015 near Connery River that flows into Hudson Bay northeast of Chesterfield Inlet (Fig. 11). They were collected at the surface of frost boils developed in till mixed with marine sediments. The two sites are at elevations of approximately 120 and 80 m asl. Single shells of *Hiatella arctica* from each sample were submitted for radiocarbon age determinations at the A.E. Lalonde AMS Laboratory (University of Ottawa). The marine shells yielded ages of 6250±50 $^{14}$C yrs BP (UOC-1674) and 6370±40 $^{14}$C yrs BP (UOC-1675), using the marine-reservoir correction of 630 years (Dyke et al., 2003). Calibrated ages are respectively 6960-7250 and 7141-7384 cal yrs BP, using the program Calib 7.1 (Stuiver et al., 2018), the Marine 13 calibration curve (Reimer et al., 2013) and a Delta-R of 285±37 years (Coulthard et al., 2010;). The complete results for the three radiocarbon dates in the region are reported in Table 1. These ages provide information about when sea level stood near their respective elevations, and also give minimum deglaciation ages for the outer part of Chesterfield Inlet. The results are discussed in Randour et al. (2016b) and Randour (2018).

*Table 1. Radiocarbon ages on marine mollusks in the region.*

| Elevation (m) | GSC sample ID | LAB ID | $^{13}$C/$^{12}$C o/oo | Conventional $^{14}$C age (BP) | Corrected $^{14}$C age (BP) for marine reservoir | Species |
|---|---|---|---|---|---|---|
| 126 | Craig, 1965 | GSC-289 | n/a | 7230 +/- 170 | 6600 +/- 170 | unidentified |
| 120 | 15MOB108A01 | UOC-1674 | +0.4 | 6880 +/- 50 | 6250 +/- 50 | *Hiatella arctica* |
| 80 | 15MOB111A01 | UOC-1675 | +0.4 | 7000 +/- 40 | 6370 +/- 40 | *Hiatella arctica* |

## ANALYTICAL PROCEDURES

### Till sample preparation

A 2-kg split of all ~3-kg regional samples was air-dried and dry-sieved in GSC's Sedimentology Laboratory, Ottawa, using a stainless steel solderless US standard No. 230 mesh screen to obtain the <0.063 mm size fraction using procedures outlined in Girard et al. (2004). The remainder (~800 g) of each 3-kg till sample was archived at the GSC, Ottawa. The large (~12 kg) till samples were shipped to Overburden Drilling Management Ltd. (ODM), Ottawa, for processing and the production of heavy mineral concentrates. Samples were disaggregated in water and screened at 2 mm to produce a non-ferromagnetic heavy mineral concentrate (NF-HMC) for picking indicator minerals, which involved a two-step process using a shaking table and heavy liquids. The oversize (>2 mm) was wet-sieved to collect the 8-30 mm fraction for lithological analysis. Sample preparation and analytical procedures for all till samples are summarized in Figure 12. The analytical and QA/QC procedures follow the protocols for till samples

collected as part of GEM projects (Spirito et al., 2011; McClenaghan et al., 2013).

**Till matrix geochemistry**

A 30 g aliquot of the silt+clay-sized fraction (<0.063 mm) of each till sample was analyzed at Bureau Veritas Commodities Canada Ltd. (BVCC) for a suite of trace, major and rare earth elements using ultratrace ICP-MS with the optional extended package for precious metals Pt and Pd, following a modified aqua regia digestion (HCl-$HNO_3$, 1:1; 95°C) (Group AQ252_EXT: 53 elements). In addition, a separate 0.25 g aliquot of the same fraction was analyzed using ultratrace ICP-MS, multi-acids digestion ($HNO_3$-$HClO_4$-HF dissolved in HCl: Group MA250: 59 elements). Another 0.2 g aliquot was analyzed for whole rock plus Cu, Mo, Ni, Pb, Sc and Zn analysis by ICP-ES, and for other trace elements by ICP-MS following a lithium metaborate/tetraborate fusion and dilute nitric digestion (LF200: 49 elements + LOI). Carbon and S were analyzed by LECO as part of the same package (TC000). Detection limits, raw analytical data and data exportable into GIS formats (less than d.l. values= ½ d.l.) are given in Appendix 4.

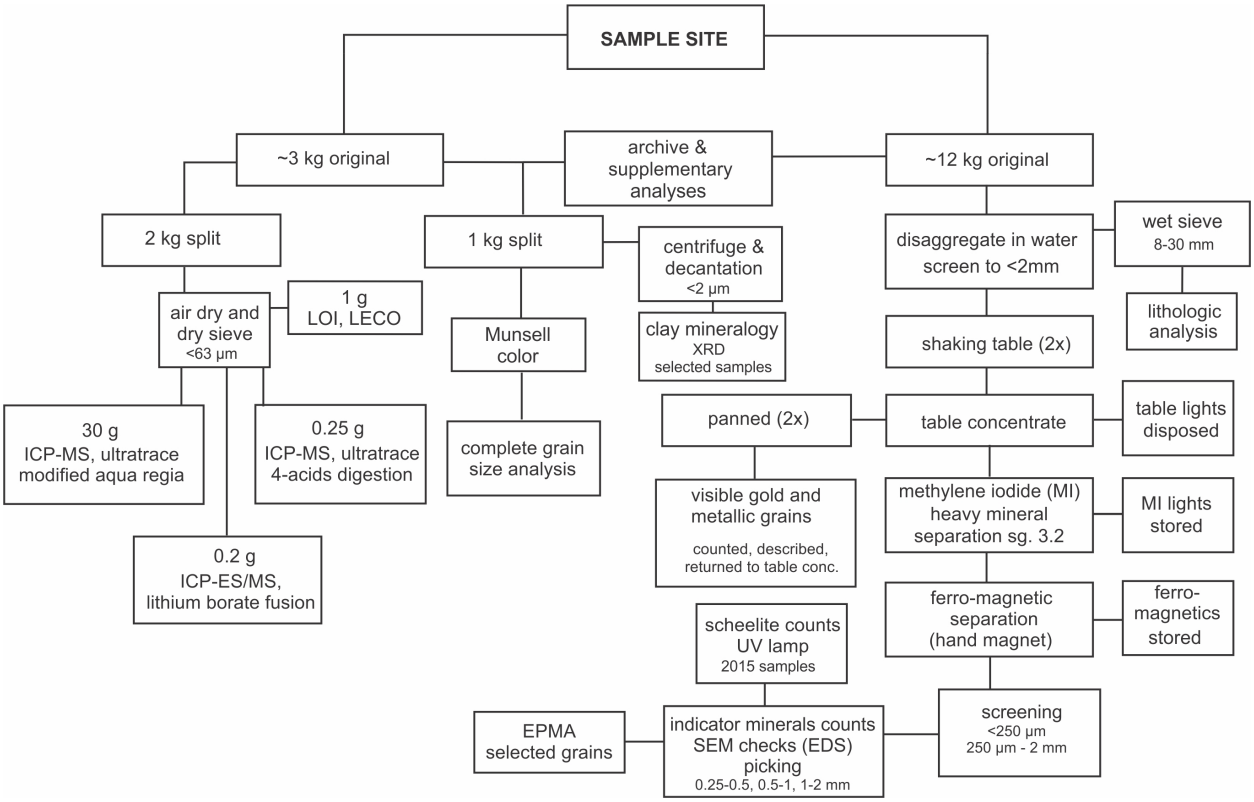


*Figure 12. Flow sheet showing steps in till sample processing.*

*Quality accuracy and quality control (QA/QC)*

Accuracy and precision of analytical data returned from commercial laboratories were determined by including analytical duplicates, primary standards (Till-4) and silica blanks (qtz-J29623) within the two sample batches submitted to the analytical laboratory in 2015 and 2016. Analysis of laboratory duplicate samples was used to monitor analytical precision of the geochemical results. Six analytical duplicates were prepared during sample preparation from field duplicate samples and were labelled with a similar sample code (e.g. 15MOB046A02 and 15MOB046B02). Analytical duplicates were inserted at the beginning of

each batch and about every 20-25 samples. Analysis of primary standards was used to monitor analytical accuracy of the geochemical results and standards were inserted randomly within each block of ~20 samples. To monitor potential cross-contamination during the sieving process and to purge the sieves between sample batches, silicic acid blanks were sieved at the beginning of each block of about 20 samples and submitted as part of the sample batch for geochemical analysis. The QA/QC statistics results discussed below are included in Appendix 4.

Precision

The results for the two laboratory duplicate samples submitted with the 2015 batch indicate that the analytical precision is very good for most elements analyzed by ICP-MS after a modified aqua regia digestion (Relative standard deviation: RSD≤10%). This method is somewhat less precise for Hf and Mo (RSD=13-16%), and even less so for Ag and Au (RSD=24% and 85%). Arsenic, B, Be, Bi, Cd, Ge, Hg, In, Pd, Pt, Re, S, Sb, Se, Ta, Te and W concentrations are near or below the lower detection limit in laboratory duplicates; therefore the precision for these elements cannot be properly evaluated. With the four laboratory duplicates analysed in 2016, precision is similar but much higher for Ag and Au (RSD=3% and 20%); and better for Bi, Cd, Hf and Mo (RSD≤20%) because concentrations are higher in the laboratory duplicates; As precision is measurable but low (RSD=44%). For the 4-acid digestion ICP-MS analyses, laboratory duplicates in 2015 indicate that the precision is also very good for most elements (RSD≤10%), but less precise for Er, Gd, Ho, Sm and W (RSD=10-20%). This method is consistently not precise for Ag, Bi, Cd and Eu (RSD>33%). Arsenic, Be, Bi, In, Lu, Re, S, Sb, Se, Tb, Te and Tm levels in laboratory duplicates are near or below the detection limit; therefore the precision cannot be properly evaluated for this method. In 2016, precision is similar but much better for Ag (12%), Bi (8%), Cd (10%), and Eu (7%); and relatively better for Er, Gd, Ho, In, Sm and W (RSD≤10%) because concentrations are higher in the laboratory duplicates; As precision is measurable but still low (RSD=36%). For lithium borate fusion and dilute nitric digestion ICP-ES/MS analyses in 2015, reproducibility is very good for the vast majority of elements (RSD≤10%). This method is somewhat less precise for Cu and MnO (RSD=10-20%), and not very reliable for Cs and W (RSD>20%). Precision for Be, Mo and Sn cannot be properly evaluated. In 2016, precision with this method is similar but higher for Cs (4%) and W (11%), and also better for Cu and MnO (RSD<4%). Carbon by LECO is reproducible (RSD<5%) while S is below the detection limit. LOI determinations are precise (RSD= 3%).

Accuracy

The accuracy in the ICP-MS analyses after the modified aqua regia digestion is good for most elements as results are generally within 10% of the mean of values from the provisional or informational analysis available for the standard Till 4. Values above 10% of the mean are shown in red in the QA/QC report Till 4 sheets in Appendix 4. Arsenic, Au, Cd, Cu, Hg, Mn and Zn were less accurate in 2015 using this method while Bi, Cd, Hg, Pb and Mn were less accurate in 2016. The accuracy in the ICP-MS analyses by 4-acid digestion was acceptable for the vast majority of elements except for Al, Mo, Te and W which were sporadically less accurate, particularly in 2015. The accuracy in the analyses by lithium metaborate/tetraborate fusion and dilute nitric digestion was good for many elements. It was less accurate for Ba, Be, Co, Eu, Mo, Nb, Nd, Ni, Sm, Sr, Ta, Tb, U, V, Y and Yb which are irregularly less reliable, specially in 2015. The silica blank qtz-J29623 returned average values of 88.35% and 88.73% $SiO_2$, and 11.5% and 10.2% LOI, in 2015 and 2016 respectively, which is consistent with previously reported values for this material (e.g. McMartin et al., 2015c; McCurdy and McMartin, 2017). The aqua regia values for Silica Sand1 inserted at the beginning of the 2016 batch was slightly elevated in Au (1.2 ppb) and in Cu

(0.63 ppm), above the expected values. There is a possibility that these higher values may be the result of cross-contamination from metal-rich samples analyzed before the batch. As and Zn (4-acids) as well as Ba, Ga, Pb (borate fusion) were sporadically very slightly elevated in some of the blanks in 2015 and 2016.

Field site variability

Results of the two regional field duplicate samples collected within 5 m of the original sample indicate that the sediment is fairly homogeneous in composition at the two sites. A full measure of the variance due to sediment heterogeneity within a site versus between sites was not completed due to the low number of field duplicate pairs (e.g. Garrett, 1983). However, the composition site variability is briefly discussed in the results section for the samples collected as field duplicates above and below the marine limit (see also Randour, 2018).

**Matrix colour and texture**

Munsell colour codes were determined on dry samples at the GSC Sedimentology Laboratory using a spectrophotometer. For textural analysis of the matrix, approximately 200-300 g of each till sample was dry-sieved to obtain the <2 mm (-10 mesh) fraction. The size classes greater than 0.063 mm were determined using wet sieving followed by dynamic digital image processing using a CAMSIZER Particle Size Analysis System. The classes of sizes smaller than 0.063 mm were determined using a Lecotrac LT-100 Particle Size Analyser. The results of the matrix colour and textural determinations for the >2 mm size fraction, sand (2-0.063 mm), silt (0.063-0.002 mm) and clay (<0.002 mm) fractions are presented in Appendix 5. The complete grain size and replicate analysis are also included in Appendix 5.

**Matrix carbon and organic contents**

Total carbon was determined on the <0.063 mm fraction with a LECO CR-412 Carbon Analyzer instrument (1350°C) (Girard et al. 2004). Only the samples with Total C > 0.10% were analyzed for inorganic and organic carbon afterwards. Loss-on-ignition (LOI), an approximation of total organic content, was determined on the <0.063 mm fraction after heating a small portion at 500°C for one hour in an ashing furnace (Girard et al., 2004). Laboratory duplicates as well as in-house (12% standard) and CANMET (Till-2, Till-4) standards were inserted for the till matrix carbon and LOI analysis. All results for the carbon and LOI analysis are given in Appendix 6.

**Clay mineralogy**

The mineralogy of the clay-size fraction (separated by centrifuge at the GSC) of selected samples was determined by X-ray powder diffraction analysis (XRD) at the Geological Survey of Canada. Mineral identification and quantitative analysis were made using EVA (Bruker AXS Inc.) software with comparison to reference mineral patterns and TOPAS (Bruker AXS Inc.), a PC-based program that performs Rietveld refinement of XRD spectra. Detailed methods and results are provided in Appendix 7.

**Clast lithology**

The >2.0 mm material from the large till samples was wet-sieved to separate the 8-30 mm fraction for lithological analysis. Pebbles were visually examined using a binocular microscope (min 48 clasts; max 200; average 187) by ODM. Pebble classes were grouped into the following three general lithological categories and counted by classes: a) Archean plutonic and high-grade metamorphic rocks (classes: 1-

granitic rocks and orthogneiss, 2-paragneiss and migmatite, 3-meta-komatiite, 4-metachert and iron formation, 5-metagabbro, 6-meta-pyroxenite and peridotite, 7-amphibolite); b) veins and tectonite (8-quartz vein, 9-shear zone); and c) unmetamorphosed Proterozoic rocks (10-sandstone, 11-volcanic, 12-syenite, 13-pyroxenite/peridotite, 14-lamprophyre, 15-diabase). Results presented in Appendix 8 include the number of clasts and the percentage (%) of the total in each category. High resolution scanned images of the classified pebbles in each sample are provided in this appendix for future reference.

**Heavy mineral processing and indicator mineral picking**

The large till samples were processed at ODM for recovery of the heavy mineral fraction and indicator mineral counting, including gold grains. Samples were processed in two separate batches (2015 and 2016 samples) in numerical order. Figure 12 outlines the sample processing flow sheet for the recovery of indicator minerals. Samples were disaggregated and sieved to obtain the <2 mm (matrix) fraction ("Table feed"), and then, processed using a double-run across a shaking table to ensure a complete recovery of all indicator minerals. The table preconcentrate was then panned for gold grains and metallic indicator minerals; after counting, these minerals were returned to the preconcentrate. After tabling and panning, the preconcentrate was further refined using heavy liquid (methylene iodide diluted to SG 3.2) and ferromagnetic (FM) separations. The <2 mm non-ferromagnetic (NFM) heavy mineral concentrates (HMC) were screened at 0.25 mm. The total number of gold, sulphide and PGM grains recovered from the panning, and the weights of table feed, table preconcentrates, NFM- and FM-HMCs are presented in Appendix 9.

Prior to indicator mineral examination and selection, the 0.25-2 mm NFM-HMCs recovered from till samples were dry sieved to 0.25-0.5 mm, 0.5-1 mm and 1-2 mm. The 0.25-0.5 mm sample fraction was further refined using a Carpco® electromagnetic separator to produce fractions with different paramagnetic characteristics to help reduce the volume of concentrate to be visually examined (Averill and Huneault, 2006). All fractions were examined under a stereoscopic microscope at ODM to determine the abundance of potential kimberlite indicator minerals (KIMs) and metamorphosed or magmatic massive sulphide indicator minerals (MMSIMs), and any other mineral indicating the presence of potential mineralization. For each sample, the entire concentrate in each of the three size fractions was examined. ODM performed checks on selected grains using SEM-energy dispersive x-ray spectrometer (EDS) to confirm mineral identification. Selected grains considered having possible KIM and MMSIM affinities were removed from the concentrate and stored in vials for further study. The 15MOB samples were later re-examined to determine the abundance of scheelite after confirmation by ultraviolet (UV) lamping of the nonparamagnetic (>1.0 amp) 0.25-0.5 mm fraction. Samples collected in the same area in 2012 (12WGA – see McMartin et al., 2013) were also re-examined for scheelite grains using UV lamping. Because of their high abundance in some samples, only a number of representative grains (max 50) of certain mineral species were picked for future analysis/archive (e.g. forsterite, bronzite, sapphirine, topaz, chromite, fluorite). Appendix 9 includes all raw grain counts from the visual identification of possible indicator minerals for the 0.25-2 mm NFM-HMCs in worksheets "KIM Counts" and "MMSIM". A summary of the MMSIM counts is presented in worksheet "MMSIM Summary".

*QA/QC*

Two blank sand and gravel samples consisting of weathered Silurian-Devonian granite (grus; i.e. Plouffe et al., 2013a,b) were inserted by the GSC at the beginning and in the middle of each sample batch (2015 and 2016) to monitor potential cross-contamination introduced during heavy mineral separation. Data

for the blank samples are listed in Appendix 9 and are highlighted in grey. Expected hornblende/titanite-zircon assemblages with no specific indicator minerals were found in the blanks. No gold, sulphides, PGMs, KIMs or MMSIMs were found in the blank samples. A comparison of the gold grain abundance between the original and the field duplicate samples indicates that gold grain counts are reproducible. The 2016 field duplicate also returned comparable PGMs, KIMs and MMSIMs grain counts while within site variability was more important in the field duplicate sample collected in 2015, especially for low Cr-diopside (5 grains versus 0), chromite (3 versus 5 grains) and forsterite (80 versus 150 grains). The 2015 duplicate sample also has one sperrylite grain versus none in the original. The variability of the KIM content between the original and the duplicate samples reflects a combination of sediment heterogeneity and the precision of the mineral separation and identification method. All picking results for the blanks and the field duplicate samples are reported in Appendix 9.

**Electron microprobe analysis**

Selected, visually identified, potential indicator minerals from the 0.25-0.5 mm and 0.5-1 mm fractions were mounted for electron microprobe analysis (EMP) on 25 mm epoxy stubs at SGS Mineral Services, Lakefield, ON, and carbon coated (total of 290 grains from 2015 samples and 438 grains from 2016). The following mineral species were mounted: Cr-pyrope, orange garnet, forsterite, chromite, ilmenite, topaz, fluorite and scheelite in 15MOB samples; Cr-pyrope, orange garnet, forsterite, chromite, Cr-diospide, low Cr-diopside and Mn-epidote in 16MOB samples. Olivine, garnet, diopside and spinel grains in selected bedrock thin sections were also analyzed by EMP (n=47). Scheelite grains were mounted but not analyzed and were archived for further studies.

Grains were analyzed at the University of Ottawa using a JEOL 8230 electron microprobe fitted with five vertical wavelength-dispersive spectrometers, in order to confirm their identity and quantify their chemical composition. Major and minor elements were analyzed under operating conditions of 20 kV accelerating voltage and 20 nA beam current, counting for 10 seconds on peak and five seconds on each background. Where possible large surface area crystals (LLIF and LPET) were employed to improve the limits of detection. Quality control data including calibration standards and analyzing crystals are given in Appendix 10. The analyzed grains were classified (or re-classified when necessary) on the basis of their chemical composition.

Approximately 8% (n=48) of the 569 potential forsterite grains from till samples were determined not to be olivine; 41 were re-classified as Cpx, 2 as low Cr-diopside, 2 as Opx, 1 as calcite, 1 as an aluminium silicate, and 1 as quartz. Of the classified 521 olivine grains, 350 have $\geq Fo_{75}$ ("Mg-rich") and as many as 171 are bona fide forsterite ($\geq Fo_{90}$). In bedrock, of the 35 olivine grains analyzed, 23 turned out to be Mg-rich ($\geq Fo_{75}$). Forsterite with ≥0.03 wt.% CaO were classified as Ca-forsterite. Two of the 5 grains picked as "Low Cr-diopside" in till samples were determined to be Cr-diopside with >0.5 wt.% $Cr_2O_3$. Low Cr-diopside were classified as having between 0.2 and 0.5 wt.% $Cr_2O_3$. Two of the orange garnet grains were reclassified as Cr-pyrope (>2 wt.% MgO). The final mineral classification and chemical data for the 0.25-2 mm and 0.5-1 mm analyzed grains are provided in Appendix 10 together with the analyzed grains from bedrock thin sections. A table reporting the total number of indicator minerals per sample and by species is also provided in Appendix 10. Based on the proportion of olivine and chromite grains confirmed after analysis ("Confirmed" column), a total number of grains per sample is given, or estimated using the average proportion of grains classified (92% for olivine). Cr-pyrope, eclogitic garnets, Cr-diopside, topaz and fluorite grains were all analyzed and confirmed.

## RESULTS AND DISCUSSION

### Till provenance

*Regional composition*

Texture

Textural data indicate that surface till in the study area has a silty sand matrix with a variable clast content; the high sand contents (33 to 92%; mean= 66%) reflect the nature of the underlying bedrock which is overwhelmingly composed of Archean felsic to intermediate plutonic rocks prone to produce sand-sized quartz and feldspar grains (Fig. 13). Regional distribution indicates low clay contents (0 to 8%; mean=3%) and moderate silt contents (8 to 65%; mean=32%). Regionally the eastern sector comprising T1 shows relatively higher sand contents than in the west (T2); this regional variation may be explained by a difference in provenance and nature of the local bedrock lithologies. The eastern sector appears to be dominated by more immature tills, derived from highly erodible, poorly resistant weathered lithologies preserved under the KID. Till texture along T2 is typically less variable than along T1 indicating less variability in the texture and composition of the bedrock lithologies within the Lunan and western Douglas Harbour domains than in the Lorillard, Gordon and eastern Douglas Harbour domains.

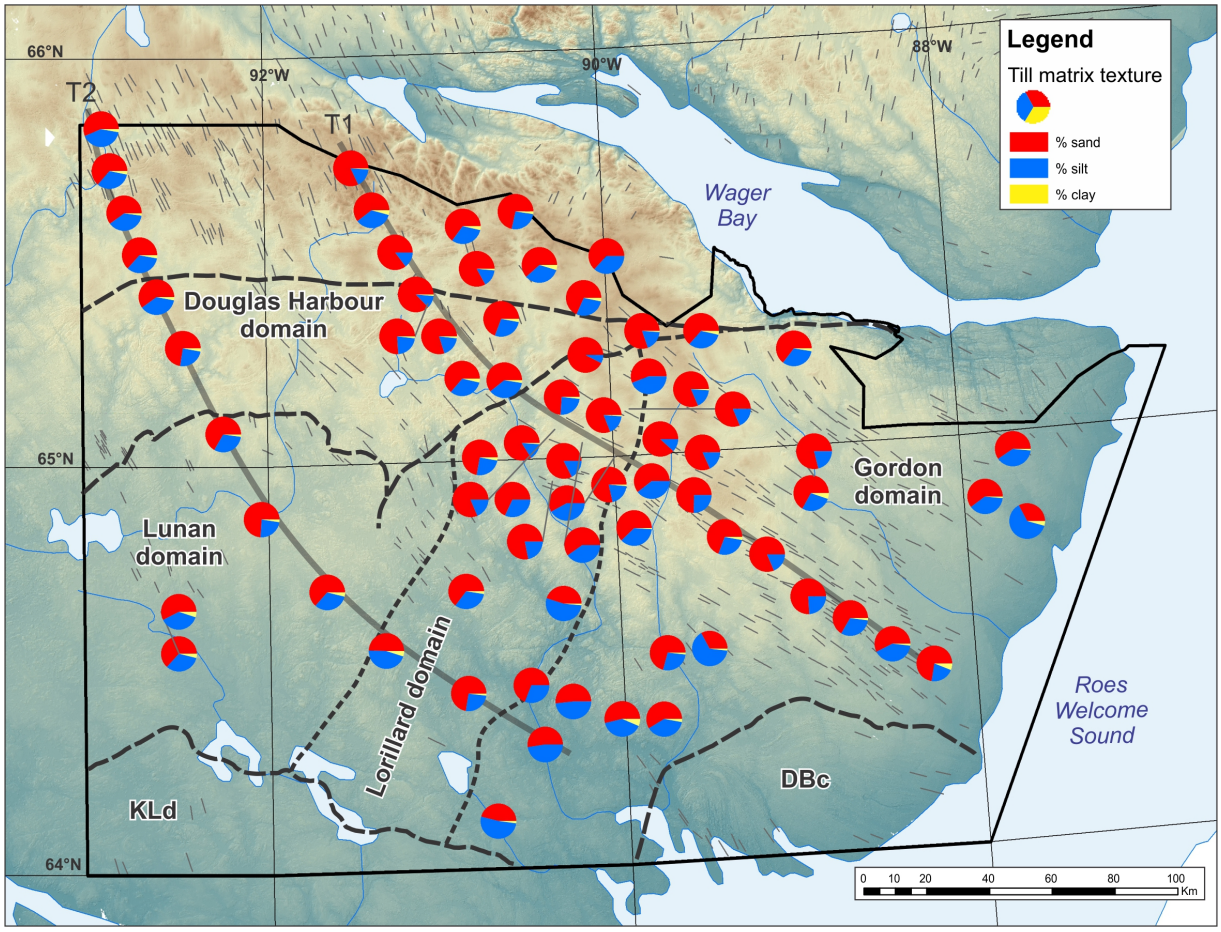


*Figure 13. Sand-silt-clay distribution in the till matrix (<2 mm) of GEM2 samples. Bedrock domains and streamlined landforms (see Fig. 6) are shown.*

High silt to clay ratios characterize the till matrix across the region but ratios are generally lower (<17.20) closer to the KID (<40 km) than further down-ice in the thick till streamlined terrain (Fig. 14). Although sandy and immature tills are located near the KID, relatively higher clay contents relative to silts

are found closer to the divide. Clay mineralogy by XRD analysis indicates samples are dominated regionally by primary plagioclase feldspar, K-feldspar and quartz with subordinate amphibole-group minerals, illite/mica and chlorite (See Appendix 7). However three till samples collected directly under the ice divide in heavily weathered terrain (15MOB034, 16MOB147 and 16MOB155) contain high proportions (>10%) of secondary minerals in the clay fraction including kaolinite, hematite and secondary mixed-layers biotite-vermiculite (e.g. hydrobiotite), and significant amorphous hydrous oxides (>40%). The presence of these secondary minerals, high amorphous material content and relatively higher clay contents in samples close to the KID supports the idea that weathering occurred during a prolonged exposure prior to the last glaciation and that it was preserved under low erosive, cold-based ice during the Last Glacial Maximum. Weathered soils in felsenmeer zones of high Torngat summits in Quebec were also interpreted as heritage from paleopedogenesis during warmer conditions than that prevailing today (Marquette et al., 2004). Below marine limit, clay and/or silt contents can be higher and more variable, reflecting uneven mixing of offshore marine sediments with till through frost churning. Winnowing by waves and currents or by the action of glacial meltwater can have a reverse effect and increase the sand content. Atypical clay contents relative to silt contents can significantly affect till geochemistry in the <0.063 mm fraction (e.g. McMartin, 2017).

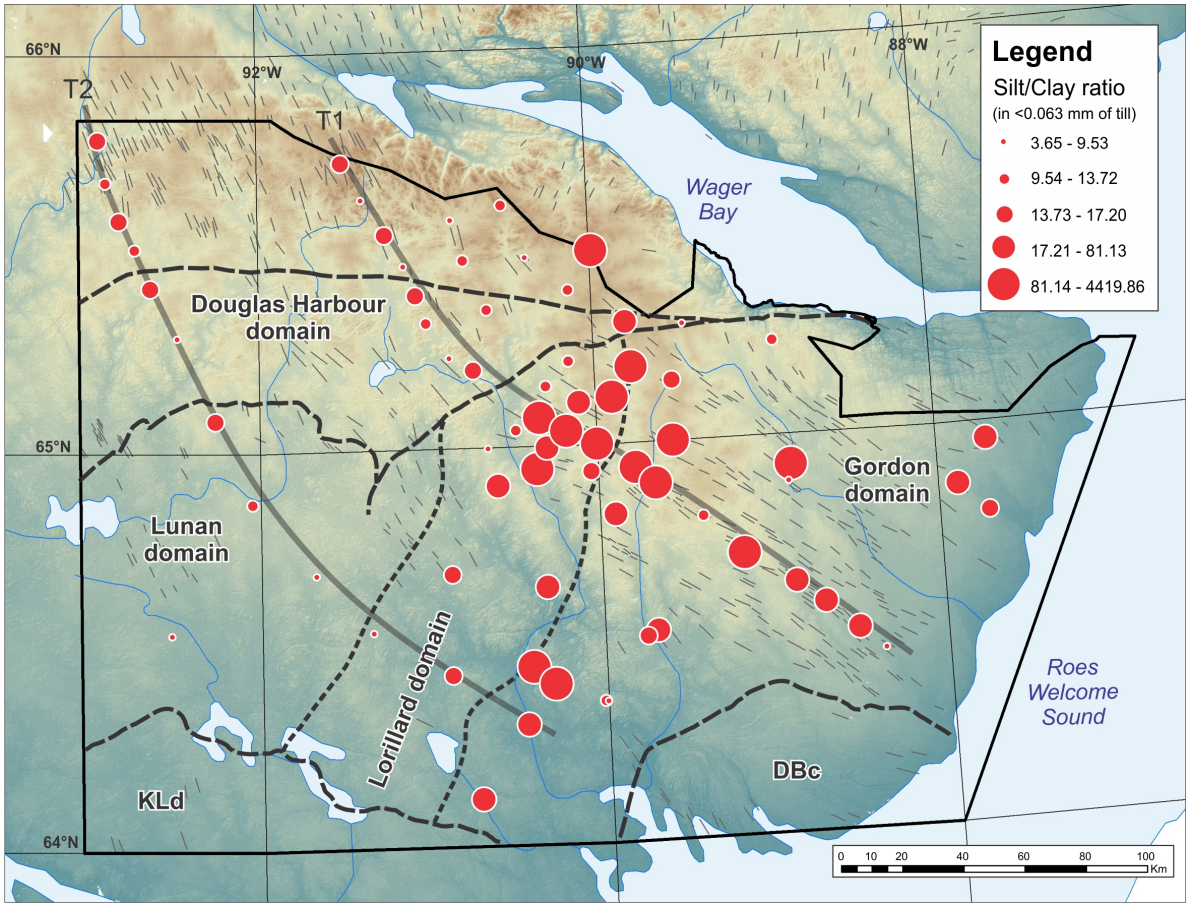


*Figure 14. Silt to clay ratio in the till matrix (<0.063 mm) of GEM2 samples. Bedrock domains and streamlined landforms (see Fig. 6) are shown.*

Clast composition

Clast contents generally indicate a local provenance; over 80% of the pebbles classify in the "undifferentiated granitic and orthogneiss" class reflecting the extensive distribution of Archean and undeformed granitoid rocks that underlie the area (See Results in Appendix 8). As no clear compositional

or textural distinction was made between the gneissic rocks across the area or across the Wager or Chesterfield shear zones (e.g. Wodicka et al., 2016), no clear variation in this class is observed in the till clast fraction. Clasts classified as "paragneiss and migmatite" are more abundant over and down-ice (SE) of the Pennington supracrustal belt and northern part of the Lorillard belt indicating the availability of local supracrustal rocks for glacial erosion (Fig. 15a). The same area shows relatively high concentrations of "deformed mafic to ultramafic clasts" (Fig. 15b), particularly amphibolite and a few meta-gabbro, -komatiite and -pyroxenite/peridotite pebbles, indicating a significant local component in till of this area. One till sample (15MOB023 - see Fig. 15b) collected directly over a Mackenzie dyke outcrop contains 5 diabase and 2 lamprophyre pebbles suggesting local glacial erosion of the dyke and of a lamprophyre, possibly emplaced along the same deep, mantle-tapping structure as the diabase.

However, depending on erodibility of the source and relative hardness of the lithology, clasts can survive glacial transport a long distance. Abundant shear zone altered clasts of brecciated meta-chert are found in several till samples down-ice (NNW) of the Quoich River fault as far as 40 km from potential sources on the north side of the KID in NTS 56F. In till sample 16MOB167 (Fig. 16; see location in Fig. 15b), directly down-ice of an outcrop identified as layered granodiorite with recrystallized shear bands (bedrock station 16WGA-S185), the proportion of shear zone altered clasts reaches 64.5%. Recrystallized quartz boulders glacially dispersed to the NNW form a striking glacial dispersal train observable from the air close to this source outcrop. On the other hand, Paleozoic carbonate clasts were only observed at the surface of till below marine limit suggesting these far-travelled erratics were transported by icebergs and not reworked from till derived from Hudson Bay. No exotic Dubawnt Proterozoic clasts were observed in till.

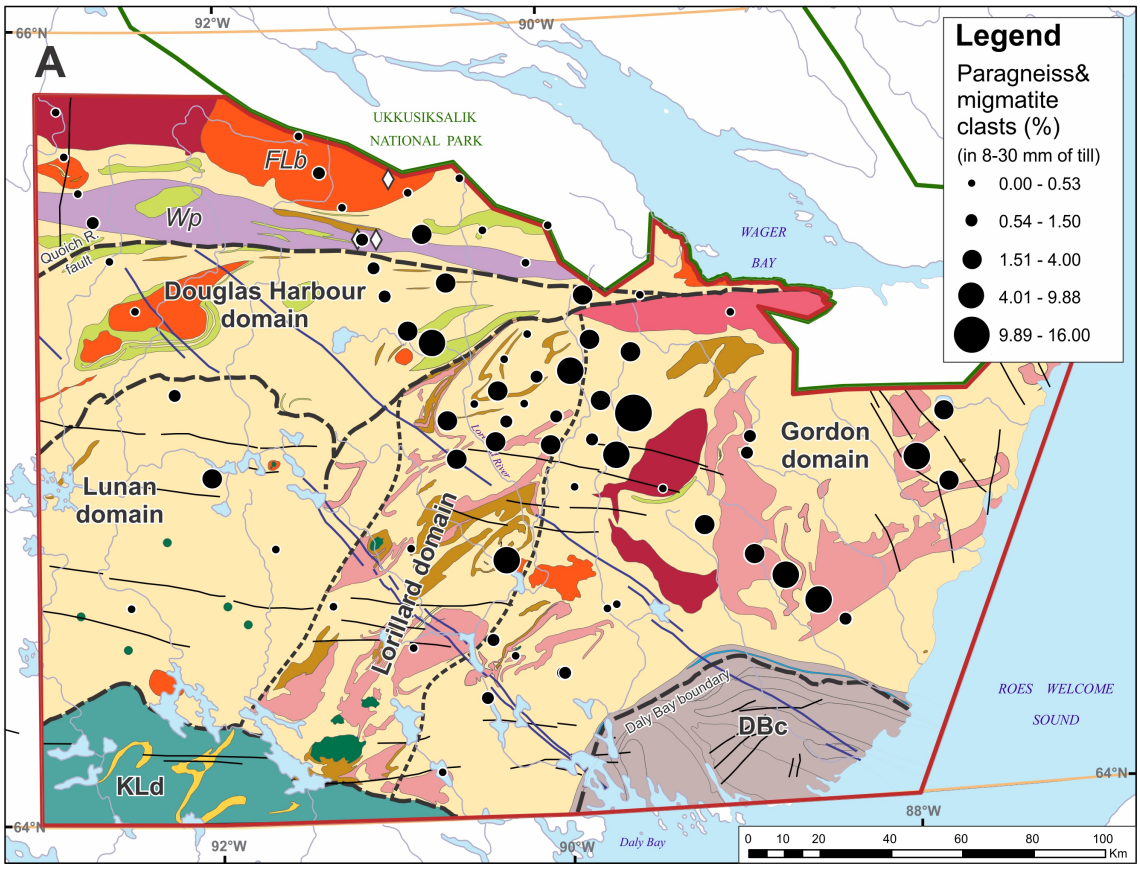

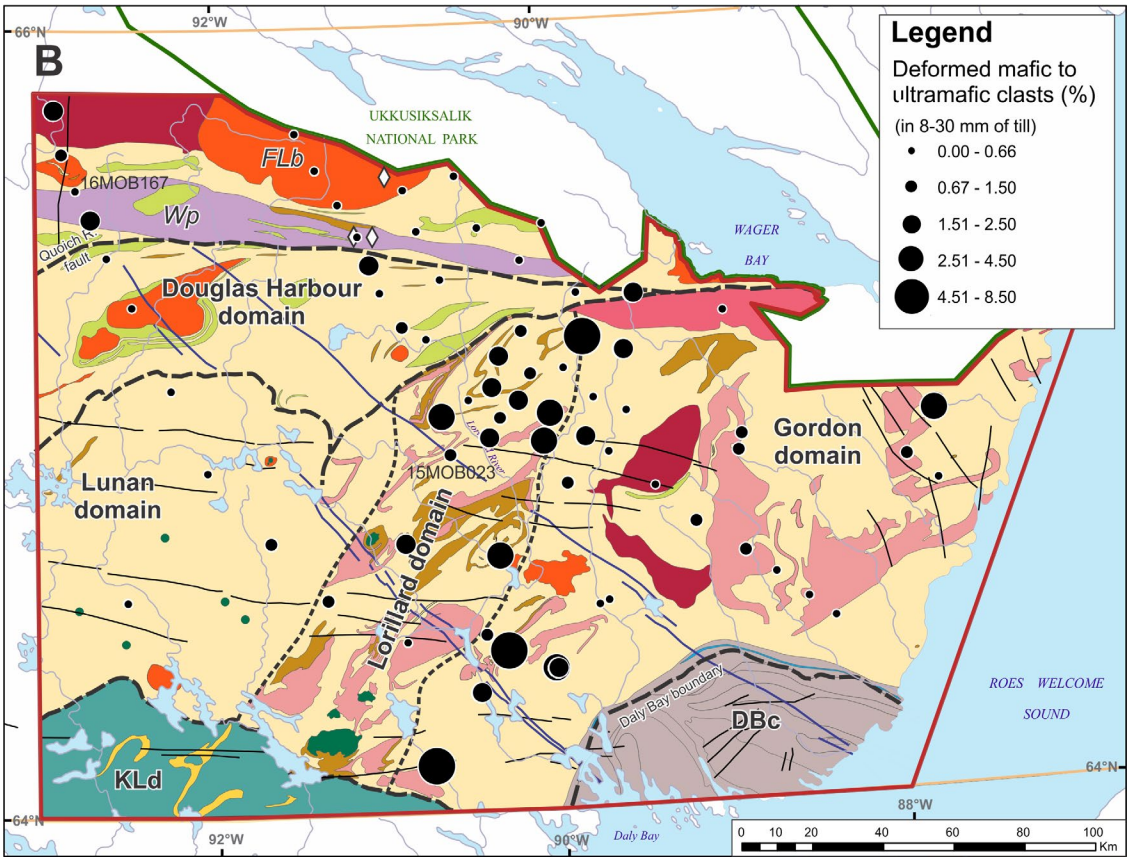


*Figure 15. Paragneiss and migmatite (A) and deformed mafic and ultramafic (B) clasts in the pebble fraction of till (8-30 mm) of GEM2 samples. Bedrock legend is given in Figure 3.*

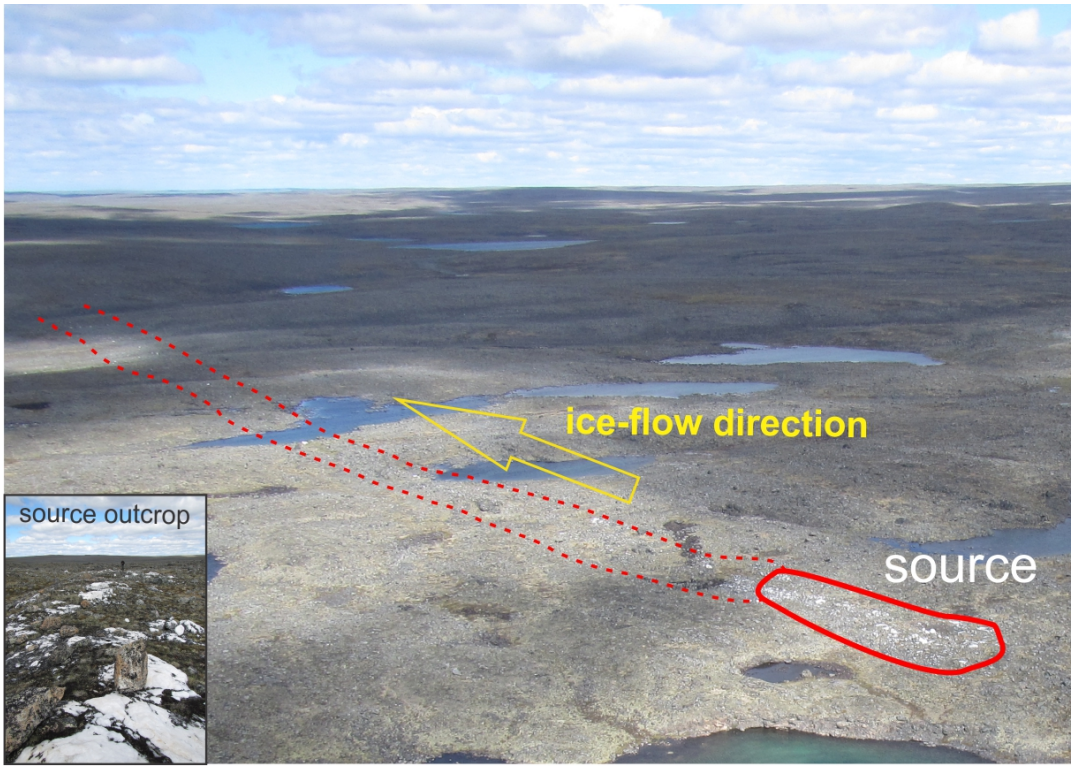


*Figure 16. Photograph from the air of ~1-km long NNW-trending glacial dispersal train of recrystallized quartz boulders from source outcrop (Site 16MOB167; bedrock station 16WGA-S185).*

Major elements

Major elements determined by lithium borate fusion/ICP-ES of the <0.063 mm fraction reflect the near complete destruction of resistive and labile minerals, hence, similar to pebble counts, may indicate regional trends related to provenance, and/or weathering. Results show that $SiO_2$ contents largely range between 60 and 70% and do not show much regional variations related to underlying bedrock domains (see Appendix 4 for entire results); $SiO_2$ contents are only slightly lower across T2 over and down-ice of the Douglas Harbour domain. $Al_2O_3$ contents are particularly constant around the mean at 15% across the region with the exception of one sample above 17% (16MOB0167 with $Al_2O_3$ at 26%). Relatively low $Na_2O$ values are found in the Douglas Harbour domain indicating lesser amounts of silt-sized primary Na-bearing silicates in the source bedrock. The relative decrease in $Fe_2O_3$, MgO, $TiO_2$, MnO and $Cr_2O_3$ with increasing $SiO_2$ contents reflects the closure of the dataset rather than changes in provenance (i.e. Grunsky, 2010). Nevertheless, increased $Fe_2O_3$ concentrations are found in gossan-rich till in the Lorillard belt, and elevated $Cr_2O_3$ contents characterize till over and down-ice of the Lorillard belt where mafic and ultramafic clasts in till were found in abundance (Fig. 17a). $K_2O$ (and to a lesser extent $TiO_2$) contents are high in till collected over and down-ice of Hudson Suite monzogranite rocks, particularly the Ford Lake Batholith (Fig. 17b), reported to have high $K_2O$ concentrations (Peterson et al., in prep.). CaO contents are uniquely low in till north of the Wager Shear zone over and down-ice of the KID perhaps reflecting the increased weathering of bedrock and resultant loss of Ca-bearing silicates in till of this area.

The chemical index of alteration (CIA) in till, used to evaluate the extent at which surface tills have weathered (Refsnider and Miller, 2010), is relatively low in the study area, varying between 47 and 56. Diluted CIA values in polythermal settings were also reported in the highlands north of Wager Bay (McMartin et al., 2015c). Only the anomalous sample 16MOB0167, rich in micaceous shear zone clasts and patchy red hematite staining, has a high CIA (74). However values are relatively high within 25 km of the KID central axis (CIA>51) suggesting till composition in this area may reflect in part erosion from weathered bedrock sources.

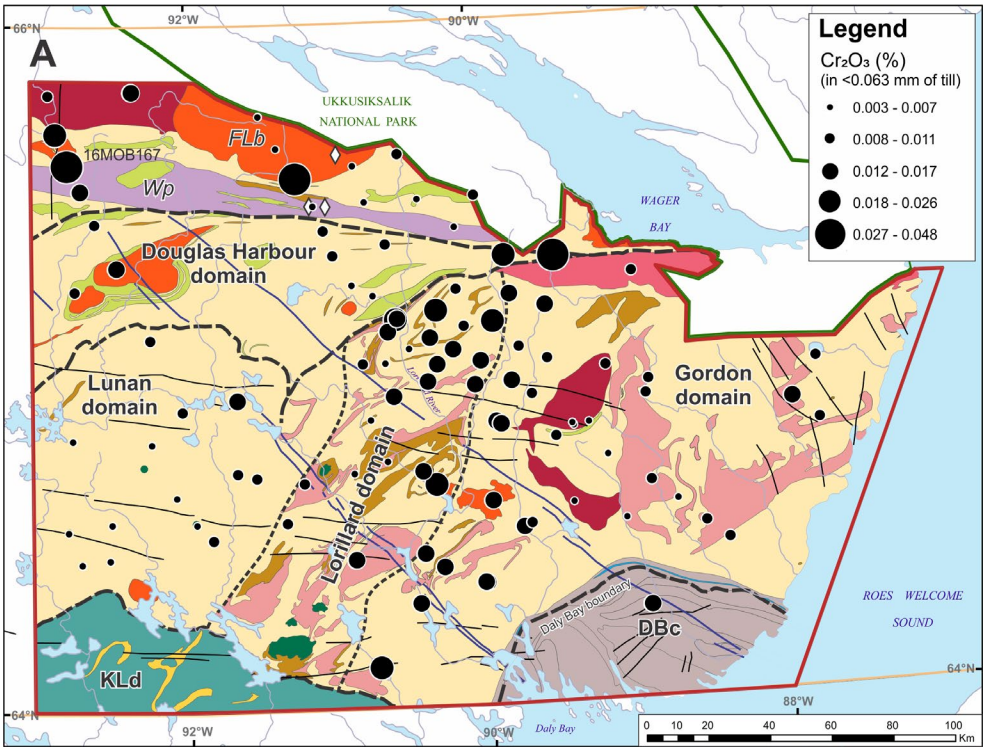

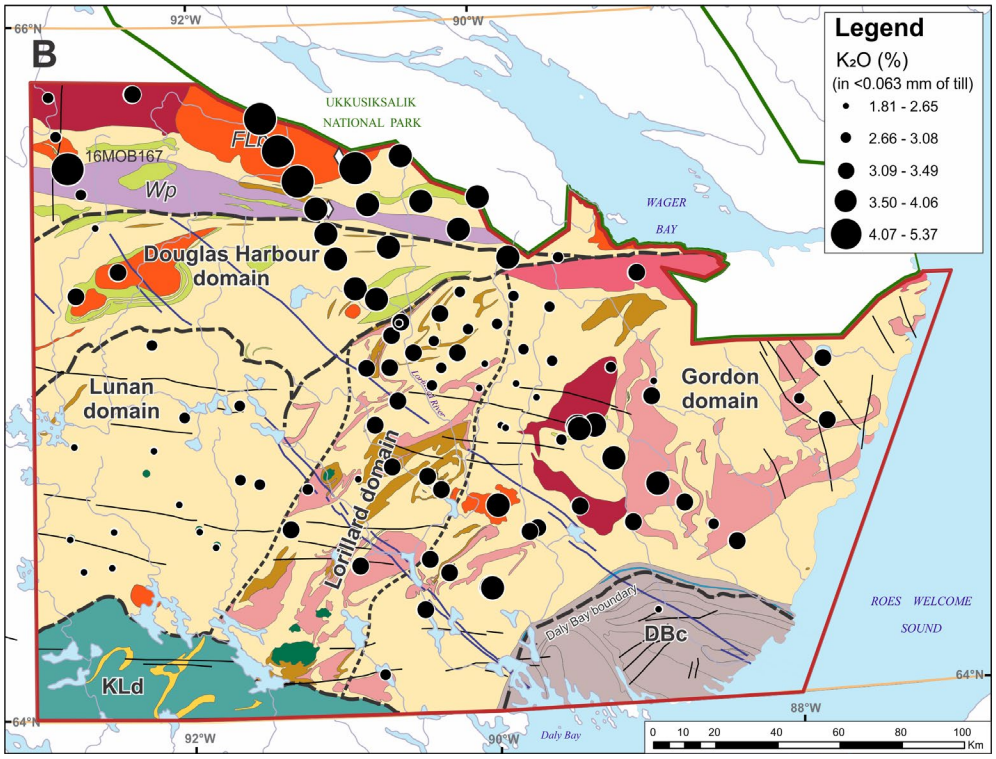


*Figure 17. $Cr_2O_3$ (A) and $K_2O$ (B) in till (<0.063 mm) of GEM1 (12WGA) and GEM2 samples. Analysis by ICP-ES/ lithium borate fusion. Bedrock legend is given in Figure 3.*

*Vertical distribution in frost boils*

Physical characteristics and the distribution of 21 selected trace and major elements were examined at two sites directly above and below the marine limit in vertical profiles (see Randour, 2018; Randour et al., in prep-2). Results indicate that till in frost boils directly below the marine limit has a relatively higher sand content and higher silt to clay ratio than till above the limit (Fig. 18); this slight sand enrichment and relative clay depletion is likely the result of winnowing by waves, not particularly apparent with field observations. Some of the variability in silt to clay ratios shown by the field duplicates exceeds the intra-profile variability but the textures follow the same trend, namely the depletion of finer particles (silt and clay) in profiles below the marine limit. Organic matter contents are higher and more variable along the profiles below the marine limit than above; matrix color also varies more along the profiles below the marine limit. Principal component analysis (PCA) on both raw and centred log-ratio geochemical datasets separate the samples by provenance (PC1) and by relative position to the marine limit (PC2) (Fig. 19). In general, till below the marine limit is slightly depleted in Ca, CaO, $SiO_2$ and Na, and enriched in Zn, Ni, Co, Fe, Al and Li, analyzed by near-total and total digestions in the <0.063 mm (silt + clay) fraction. Higher organic contents may explain some of the elemental enrichments in till below the marine limit, while the loss of fine particles may also influence elements held in silt- and clay-sized minerals, depending on the site. Therefore, it appears that marine reworking slightly modifies till composition near the marine limit as a result of changes in texture and the resulting mineral partitioning. Higher porosity, weathering and organic matter contents may also affect composition in reworked till below the marine limit. However, provenance remains the dominant factor controlling till composition and can explain ~80% of the variation at these two sites (Fig. 19). Moreover, the geochemical variations observed down-profile above and below the marine limit may be frost boil specific and reflect incomplete and variable mixing by cryoturbation processes.

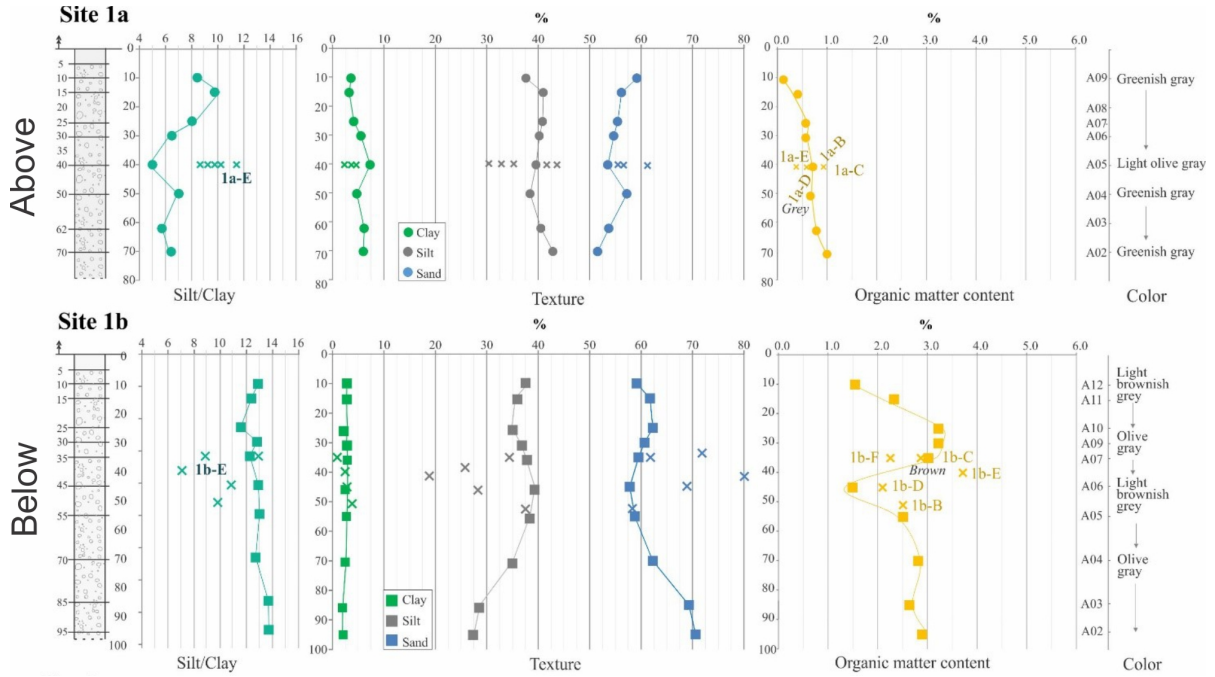


*Figure 18. Physical properties in till vertical profiles at Site 1 (a= above marine limit; b= below marine limit). The first profiles show the silt/clay ratios; the second grain size results; the third the organic matter contents (LOI %). The last column gives the color of till in the frost boil samples (from Randour, 2018). Sample depth is in cm on the left side. Results of the field duplicates are indicated by a cross (and sample number).*

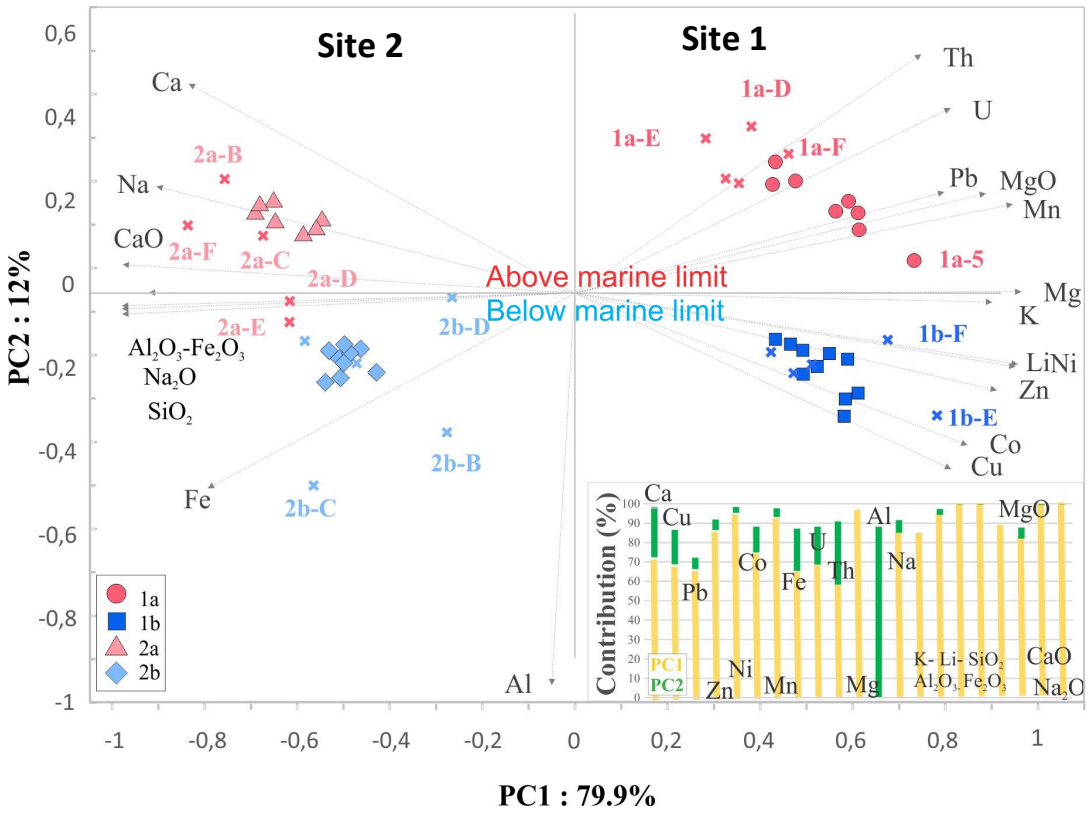


*Figure 19. Principal component analysis biplot graph (centred-log data). Inset graph shows the score contribution for PC1 and PC2 (from Randour, 2018). Location of Sites 1 and 2 are indicated on Figure 11. Field duplicate samples are indicated by a cross (with sample number); geochemical composition of the field duplicates also permits the separation of the samples by provenance and by relative position to the marine limit.*

**Implications for mineral potential**

*Diamonds*

The distribution of potential KIMs in regional surface tills suggests glacial dispersal from diverse ultramafic and mafic bedrock sources: the Nanuq kimberlite field, peridotite and amphibolite bodies within the supracrustal belts, undeformed ultrapotassic mafic intrusions, and possibly unknown kimberlite. The distribution of forsteritic olivine ($Fo_{\geq 90}$) alone does not permit differentiation of the various olivine-rich mantle sources in the region (Fig. 20). CaO, NiO and MnO contents in forsterite have been used to differentiate mantle from magmatic olivine (e.g. Koller and Brey, 1990; Arndt et al., 2010). Specifically, low CaO (≤0.1 wt.%) and MnO (≤0.15 wt.%), as well as high NiO (≥0.3 wt.%), generally characterize forsteritic olivine in mantle peridotite (Bussweiler et al., 2017). In addition, CaO contents of kimberlitic olivine are typically higher than 0.02 wt.% (Foley et al., 2006; Zheng et al., 2006). In the study area, olivine from Archean peridotite bodies have low Mg# and low CaO (<0.03 wt.%) and high NiO (>0.4 wt.%) (Fig. 21-22). All forsterite grains with ≥0.03 wt.% CaO have 0.30-0.40 wt.% NiO and 0.07-0.20 wt.% MnO (see Appendix 10 for complete results), therefore CaO can be used as an indicator element for olivine in mantle xenoliths collected from kimberlite ("Ca-forsterite").

The distribution of Ca-forsterite, eclogitic garnet and Cr-pyrope forms a ~60 km SSE-trending zone parallel to the dominant ice flow, down-ice from the Nanuq kimberlites (Fig. 23). A small number of Cr-diopside (Mg# ≥90) and chromite grains are also found in a few samples within the same area. Single grains

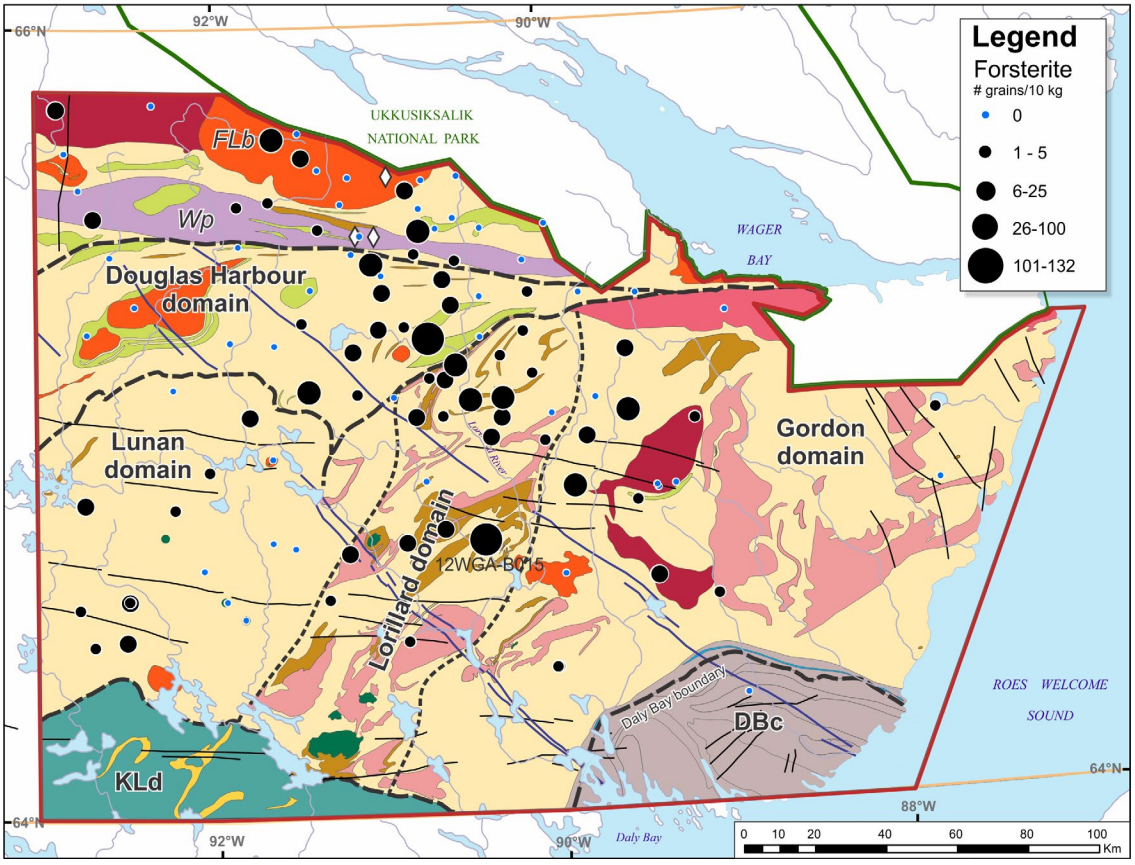


*Figure 20. Distribution of total forsteritic olivine counts (Fo ≥90) in GEM1, GEM2 and 2004 GSC till samples. Total forsterite counts for GEM1, 2016 GEM2 and 2004 samples are confirmed based on a selection of analyzed grains. Not all 2015 GEM2 samples were analyzed by EMP for olivine; counts for these samples are estimated using the average proportion of grains classified as olivine in the analyzed grains (92%). Bedrock legend is given in Figure 3.*

of Cr-pyrope (G9) are dispersed further to the SE within the streamlined till that extends to the coast and are likely the result of re-entrainement and long distance transport from the Nanuq kimberlites. The distribution of this restricted set of KIMs in regional till encompasses the two SSE-trending ~50 km-long dispersal trains from the Nanuq kimberlites (Pell, 2008): 1) a ribbon-shaped train trending 155° from the westernmost kimberlite (Kayuu Tudlik) to the Chesterfield shear zone, dominated by Cr-pyrope, eclogitic garnet and chrome diopside with some forsteritic olivine and chromite, and 2) a less well-defined, more fan-shaped train trending ~150° from the easternmost kimberlite (NQN001) with mainly Cr-pyrope grains. High counts of Ca-forsterite (n=18) at site 12WGA-B015 in the Lorillard domain are likely not related to dispersal from the Nanuq kimberlites (see Fig. 23 for location); the total counts of grains in this sample remains unconfirmed as it is estimated from a single grain of Ca-forsterite analyzed out of 22 olivine grains, and extrapolated based on a total count of 400 Mg-rich olivine grains. This sample also lacks any other KIMs. However, a certain potential for unknown kimberlite cannot be completely discounted in this area since other KIM grains (Cr-pyrope with alteration mantle and Mg-ilmenite) were found in stream sediments along the Lorillard River between the tail of the Nanuq kimberlite dispersal train and site 12WGA-B015 (Day, pers. comm.).

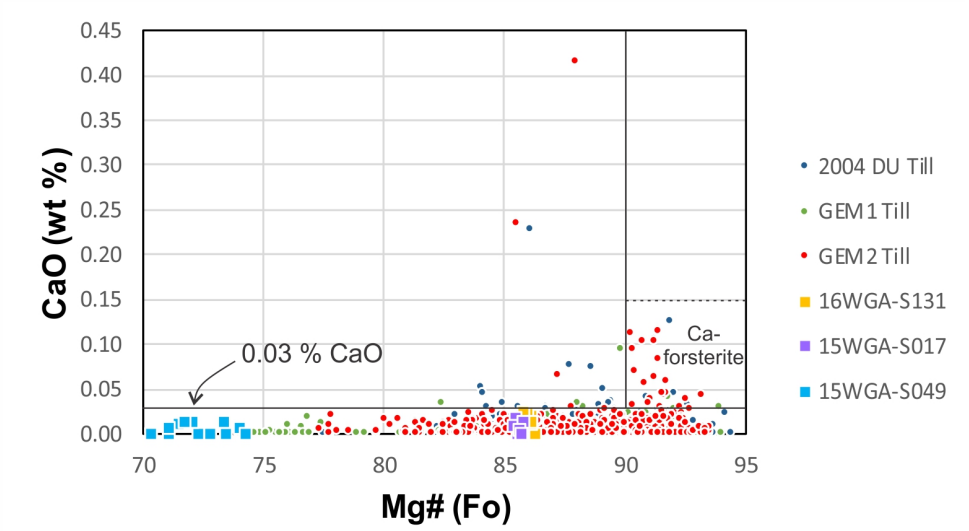


*Figure 21. CaO vs Fo in olivine grains (confirmed after EMP analysis) from GEM2 (n=521), GEM1 (n=281) and 2004 DU (n=294 grains) till samples. Olivine from three potential bedrock sources were also analyzed by EMP (altered peridotite from Lorillard belt: S131 and S017, and Meen Lake layered intrusion: S049).*

Relatively elevated concentrations of forsterite grains also occur in till collected over the Lunan domain (Fig. 20). Specifically 3 Ca-forsterite, 6 Cr-diopside (Mg#>90) and possibly 2 omphacitic diopside grains are found in samples located in the southwestern part of this area, collected near or directly over underformed pyroxenite bodies (see Fig. 23 for location; 12WGA-B006, M001, M002, 16MOB177&178). The majority of the olivine grains in these samples consists of forsteritic olivine with <0.03 wt.% CaO, and the low-Cr diopside grains contain generally too little $Na_2O$ and $Al_2O_3$ to be omphacitic diopside from eclogitic assemblages (McCandless and Gurney, 1989; See Appendix 10 for complete results). Hence the source(s) of the forsterite and diopside grains in these samples is thought to be largely derived from local pyroxenite rather than unknown kimberlite. Two Ca-forsterite and four omphacitic diopside grains were also recovered in a number of samples further to the NE (04DU070, 12WGA-B017 and 16MOB173); diamond potential is unsure in this area, although one eclogitic garnet (G4) was found in sample 16MOB173

(Fig. 23). Coronitic gabbro bodies and possible eclogite are located southeast of Lunan Lake in the Lunan domain (A.N. LeCheminant, pers. comm. 2016).

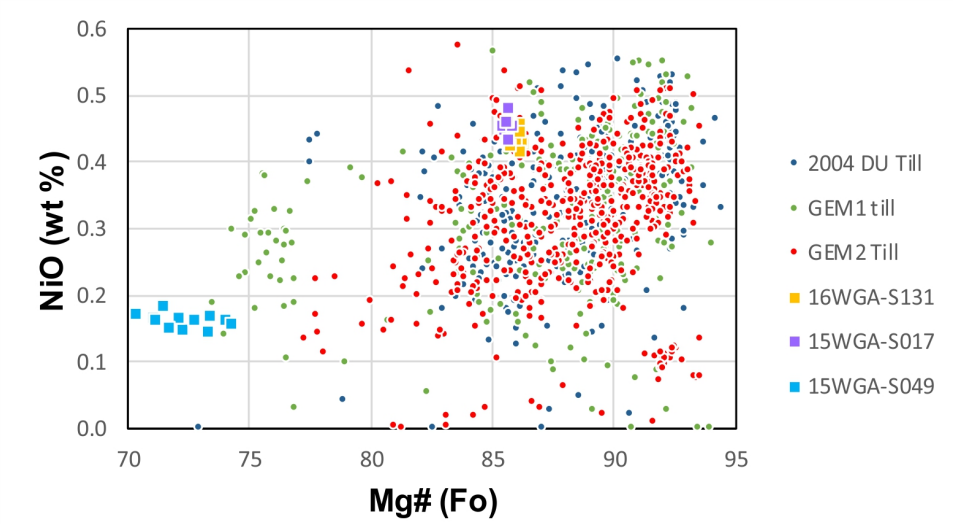


*Figure 22. NiO vs Fo in olivine grains (confirmed after EMP analysis) from GEM2 (n=521), GEM1 (n=281) and 2004 DU (n=294 grains) till samples. Olivine from three potential bedrock sources were also analyzed by EMP (altered peridotite from Lorillard belt: S131 and S017, and Meen Lake layered intrusion: S049).*

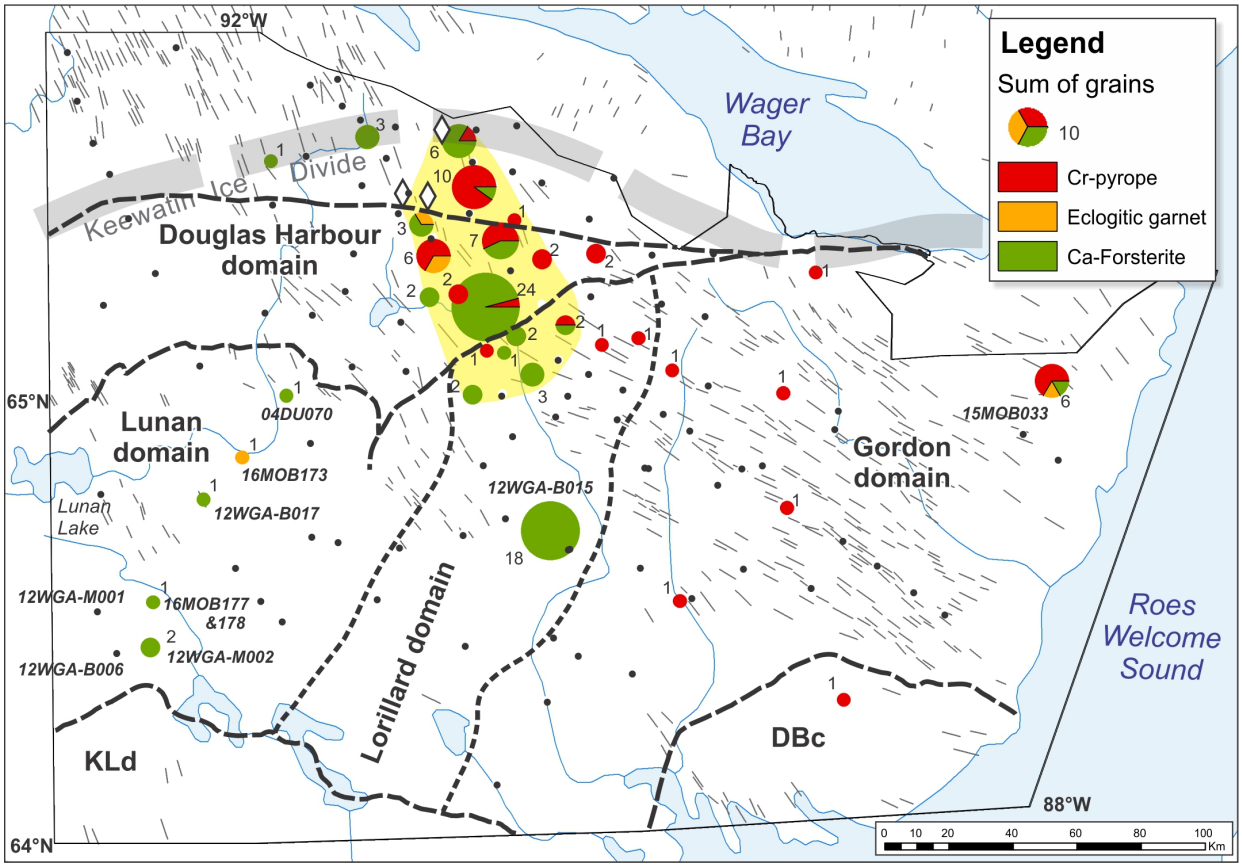


*Figure 23. Distribution of KIMs (Cr-pyrope, Eclogitic garnet and Ca-Forsterite) in GEM1, GEM2 and 2004 GSC till samples. Regional dispersal train of multiple KIMs from the Nanuq kimberlites is indicated in yellow. Bedrock domains and streamlined landforms (see Fig. 6) are shown.*

More favorable in terms of diamond potential is the presence of multiple KIMs with kimberlitic composition in sample 15MOB033 south of Meen Lake in the Gordon domain (Fig. 23). The presence of four Cr-pyrope (peridotitic G9 and megacrystic G1), one eclogitic garnet and one Ca-forsterite, in addition to potentially 16 low Cr-diopside and 15 bronzite grains (not analyzed by EMP), suggests a clear potential for a kimberlitic source up-ice (northwest) of the sample (Fig. 24). Proximity to the source rock is indicated by the preservation of a kelyphite rim on a 0.5-1 mm large Cr-pyrope grain (G9) and the presence of Mg-rich serpentinized peridotite pebbles with olivine macrocrysts in the pebble fraction. Diamond preservation potential is shown by the coincidence of 3 picroilmenite having kimberlitic affinities (Fig. 25a). Note that the composition of olivine in this till sample ($Fo_{78-92}$) is unlike the one found in olivine ($Fo_{70-74}$) from the underlying coronitic ultramafic layered intrusion (15WGA-S049 - see Fig. 22).

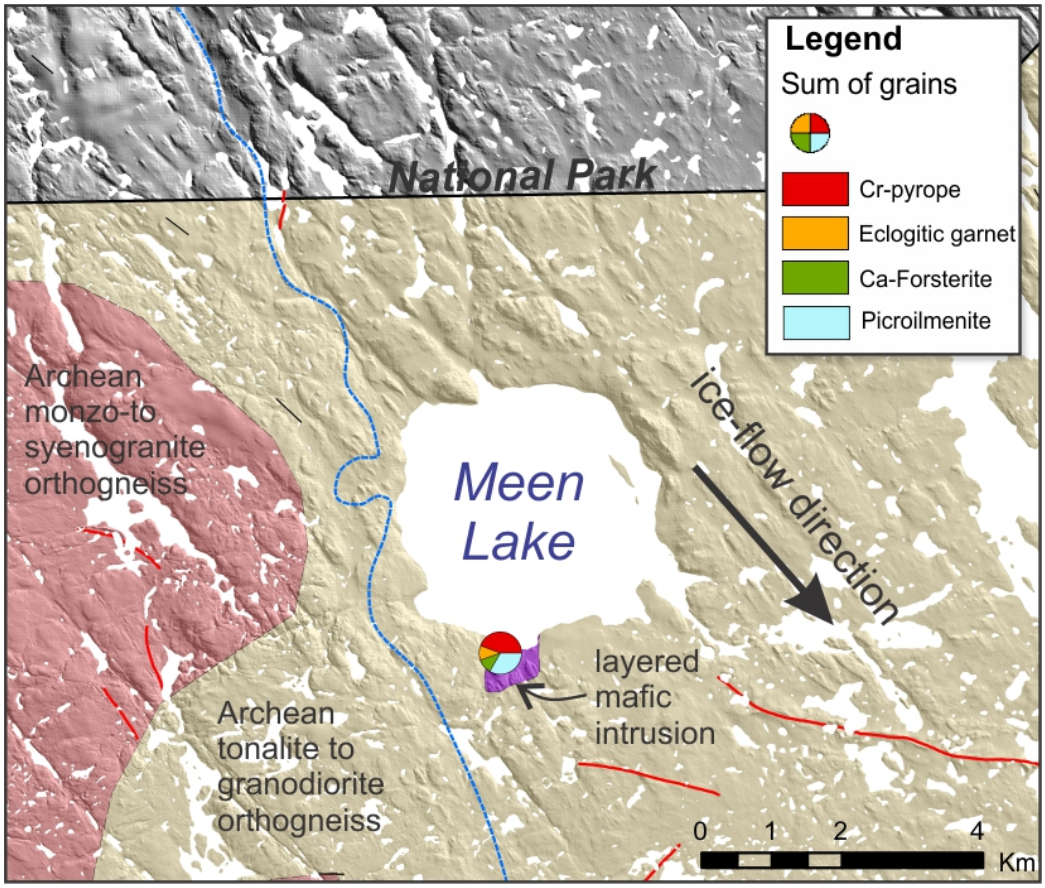


*Figure 24. Geological setting for sample 15MOB033 south of Meen Lake (see location on Fig. 23). Nine KIM grains confirmed after analysis by EMP (4 Cr-pyrope, 1 eclogitic garnet, 1 Ca-forsterite and 3 picroilmenite) were found in this sample. Marine limit (blue dashed line) and eskers (red line) are shown. Ice-flow direction is derived from measured striations and streamlined landforms.*

Till geochemistry of the matrix fraction is not particularly useful in the region to map out glacial dispersal from the Nanuq kimberlites. Only a few incompatible elements, such as Hf and Zr, which can be useful pathfinder elements for diamond exploration (i.e. McClenaghan and Kjarsgaard, 2007), have relatively high concentrations in the till matrix (<0.063mm; quenched fusion) down-ice of the Nanuq kimberlites, mimicking the KIMs dispersal train to some degree. Scattered sources of alkaline intrusions and/or ultramafic rocks probably dilute the potential geochemical signatures of kimberlite in till and create poorly developed geochemical dispersal trains.

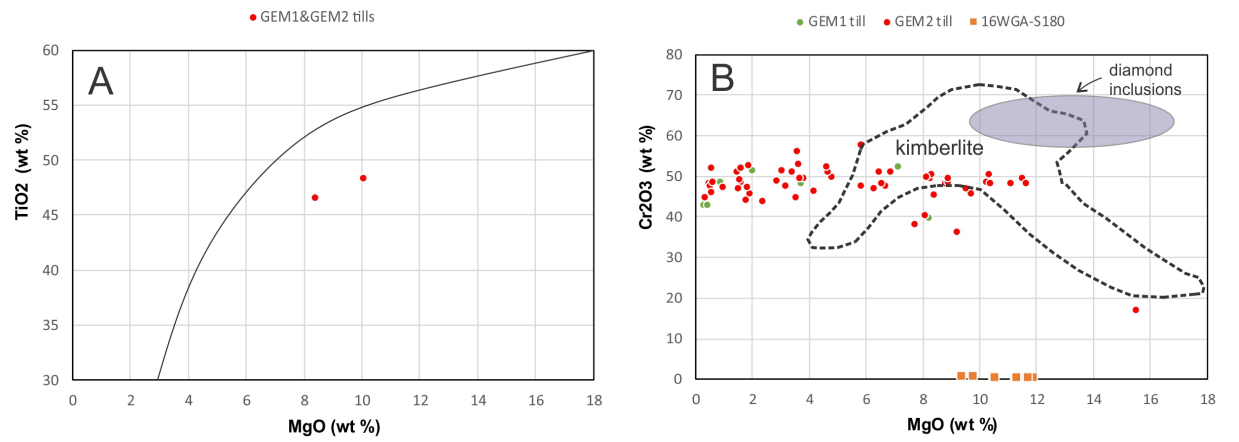


*Figure 25. a) MgO vs $TiO_2$ in ilmenite from till sample collected at Meen Lake (15MOB033: 3 grains). b) MgO vs $Cr_2O_3$ in all chromite and spinel grains (confirmed after EMP analysis) from GEM1 (n=7 grains) and GEM2 (n=57 grains) samples. Spinels (n=9) from a peridotite in the Douglas Harbour domain (S-180), were also analyzed by EMP. The curve for the $TiO_2$ plot separates crustal ilmenite (left) from kimberlitic ilmenite (right)(after Wyatt et al., 2004). Dashed line on the $Cr_2O_3$ plot includes chromite from worldwide kimberlite localities while the ellipse includes chromite from diamond inclusions (after Nowicki et al., 2007).*

*Ni-Cu, PGEs and chromite*

The potential for Ni-Cu, PGEs and chromite mineralization in the region mainly lies in Archean komatiite/pyroxenite/peridotite ultramafic bodies common in supracrustal panels of the Lorillard domain. Abundant Mg-rich olivine grains in till, including forsterite (but with CaO contents <0.03 wt.%), form a large SE fan-shaped dispersal train partly overlapping the tail end of the Nanuq dispersal trains in the Lorillard domain (Fig. 20). This anomalous area reflects palimpsest glacial transport in south to southeast directions for as much as 60 to 100 km from potential sources in the Lorillard belt. The large number of coarse-grained Mg-rich olivine (0.5-1 mm), olivine chemistry and the presence of meta-komatiite pebbles (intrusive peridotite and pyroxenite phases) suggest local sources of olivine-rich mantle rocks, such as peridotite bodies within the Lorillard belt, as confirmed by the composition of olivine in bedrock samples from this belt (Figs. 21&22). Layered intrusions and marble may also be potential sources of forsteritic olivine in the general area and within the Douglas Harbour domain. High Pt and Pd values in the till matrix seem to be associated with till samples rich in forsterite only, up-ice from the start of the chromite anomalous area described below. Ni-Co-Cr concentrations in the till matrix of this area are generally high but not the highest of the till datasets (see Appendix 4).

The distribution of chromite grains, unlike that of forsterite, is restricted to the northeast part of the Lorillard belt forming a relatively short (<30 km) SE dispersal train, suggesting the source for the chromite grains is clearly distinct from the Nanuq kimberlite bodies, and from the other mafic to ultramafic sources rich in forsterite only (Fig. 26). Composition of these chromite grains does not suggest a diamond affinity although some of the grains plot in the kimberlite field of Nowicki et al. (2007) (Fig. 25b). Many grains from this area are large (0.5-1 mm) and classified as AM chromite (aluminomagnesium) suggesting a local source in mafic to ultramafic bodies not yet mapped amongst the Archean tonalite to granodiorite gneiss of the Lorillard and adjacent Gordon domains. Interestingly, all the speryllite grains (n=5) found in the entire till datasets are located within the chromite anomaly. A significant number of chromite grains were also found in stream sediments directly downstream of the till chromite anomaly (Day, per. com). The highest potential for Ni-Cu-PGEs-chromite mineralization therefore lies over the heavily drift-covered eastern part of the northern Lorillard belt, in undefined mafic to ultramafic rocks.

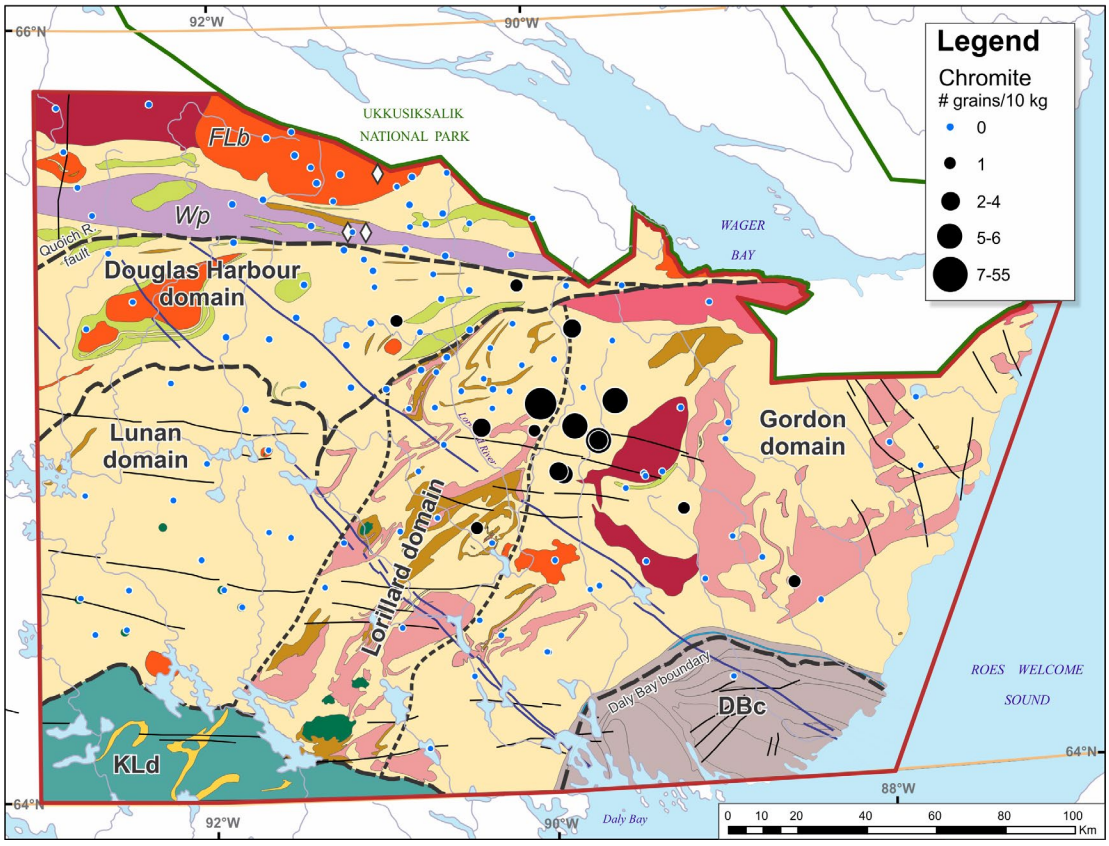


*Figure 26. Distribution of chromite grains in GEM1, GEM2 and 2004 GSC till samples. Bedrock legend is given in Figure 3.*

*Precious and base metals*

Elevated to moderate concentrations of base and precious metals (i.e. Ag, Cu, Bi, Mn, Hg, Au), MMSIMs (Mn-epidote, red rutile, ±corundum, ±sapphirine; Fig. 27) and gold grains were found in gossan-rich till as well as over and down-ice of supracrustal rocks within the northern part of the Lorillard domain. The presence of these elements and minerals indicates the potential of this area to host base- and precious metal mineralization. Several sulphide-rich boulders were found at the surface of till immediately (<1 km) down-ice of mapped mineralized outcrops and gossans in the Lorillard domain (McMartin et al., 2015a, 2016b).

Smaller gossanous horizons were mapped in several other supracrustal panels north of the Chesterfield shear zone. Coloured spinel grains and red rutile (not chemically analyzed), potentially indicative of hydrothermal alteration associated with metamorphosed VMS deposits (e.g. Averill, 2001), are abundant on either side of the Quoich River fault in NTS 56F (Fig. 27). Cu-Zn contents in till are relatively high in the same area (21-75 ppm Cu and 79-102 ppm Zn by 4-acids). A till sample collected southeast of Lunan Lake also contains 50 coloured spinel grains of unknown origin together with 21 corundum and 13 red rutile grains (12WGA-M007). Thin section examination of the nearby coronitic gabbro bodies revealed similar mineralogy with spinel, rutile, and possible corundum (A.N. LeCheminant, pers. comm. 2016).

Sample 15MOB018 in the central part of the Lorillard domain (see location on Fig. 27) contains 7 chert/iron formation pebbles with characteristic orange spessartine garnet, the Mn-rich variety commonly associated with Archean volcanogenic Au-Ag-Zn sulphide deposits or metamorphosed Mesoproterozoic

Zn-Pb-Ag sulphide deposits (S. Averill, per. com.). One of the 7 garnetiferous pebbles is a coticule rock that is used as a vector for VMS deposits. This sample also yielded 20 bronzite, two spessartine/Mn-almandine, one red rutile and one ruby corundum in the heavy mineral fraction. Potential bedrock sources for this anomaly include iron formation and garnetite within the Lorillard supracrustal belt.

Particularly high counts of topaz (n=569), scheelite (n=18) and gold (n=8) grains, as well as the highest W and Sn contents of the entire till datasets (3.7 ppm W and 6 ppm Sn by borate fusion), are found in one locally-derived till sample over the KID (15MOB034; Fig. 27). This suggests some potential for skarn or greisen mineralization in the Pennington supracrustal belt within the eastern part of the Douglas Harbour domain north of the Wager shear zone. Clasts composition of this sample consists of angular mono-lithologic leucogranite pebbles indicating the diamicton collected under the ice divide is the result of mixing by frost-heaving (felsenmeer) and long-term, in situ weathering.

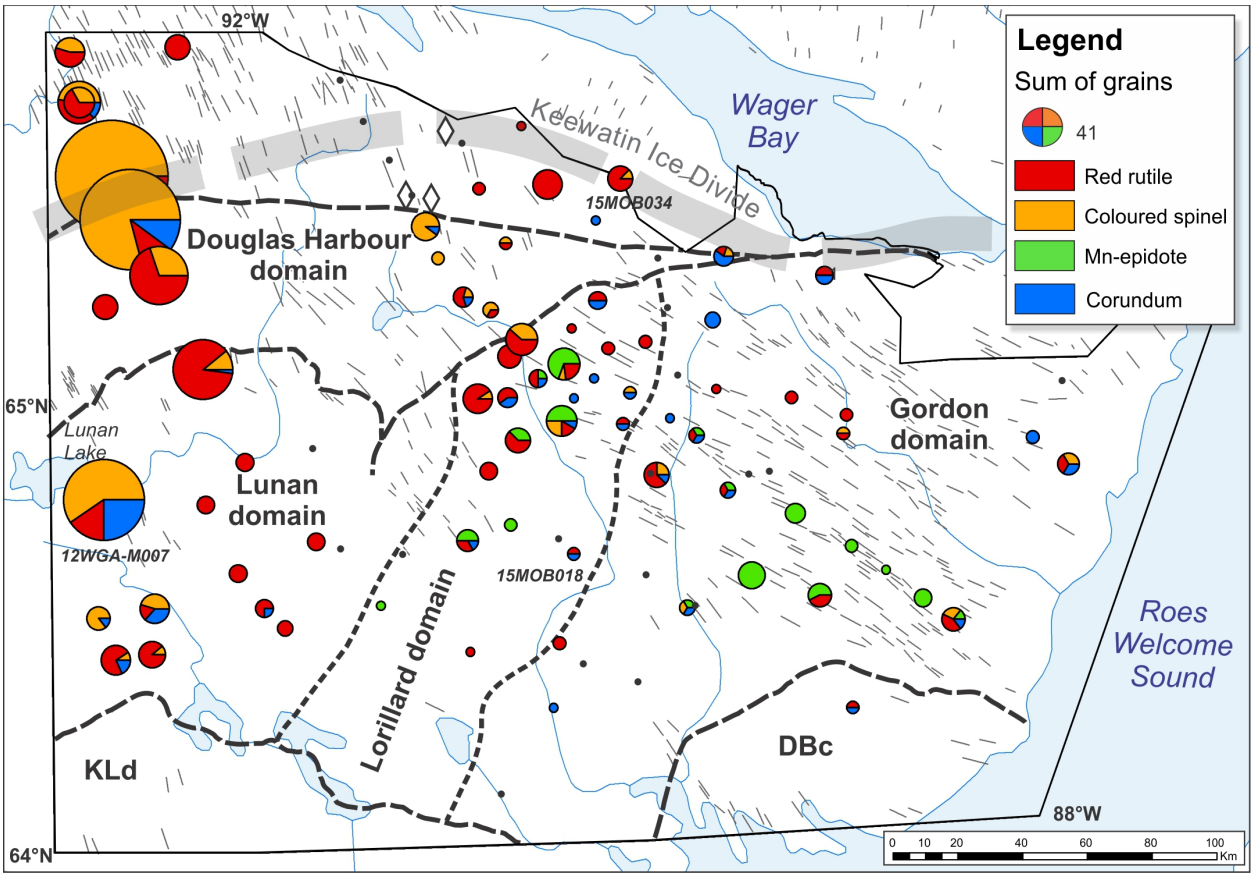


*Figure 27. Distribution of selected MMSIMs (Mn-epidote, red rutile, corundum and coloured spinel) in GEM1 and GEM2 till samples. Bedrock domains and streamlined landforms (see Fig. 6) are shown.*

## SUMMARY

The Geological Survey of Canada completed targeted surficial geology studies and till sampling south of Wager Bay in mainland Nunavut as part of the Geo-mapping for Energy and Minerals (GEM-2) Tehery-Wager Activity of the Rae Project. The results of this activity provide an improved Quaternary geological framework that will support the mineral exploration industry. This Open File report presents an overview of the regional surficial geology and integrates surface till composition from GEM-1 and GEM-2 till surveys as well as previous GSC till surveys to evaluate mineral potential. It releases the complete

field database and analytical results from the 2015 and 2016 field seasons as well as metadata for the survey (Appendix 11).

Quaternary field observations were recorded at 202 field stations; 80 of these included ice-flow indicator measurements. Regional surface till samples were collected at 73 sites to provide more detail on geochemical anomalies identified in 2012 as part of GEM-1, support bedrock mapping in areas of thick drift and characterize glacial transport along two 200 km-long transects across the Keewatin Ice Divide. Regional samples were primarily analyzed for matrix geochemistry and indicator mineral analysis of the sand fraction. A total of 54 till samples were also collected in vertical profiles and analyzed for geochemistry at two sites to evaluate the effects of marine reworking on till texture and geochemical composition. The surface of bedrock and boulders was collected at 13 sites for terrestrial cosmogenic nuclide (TCN) dating; marine mollusk shell samples were collected at 2 sites for radiocarbon age determination.

Field observations indicate this region is important for the glacial history reconstruction of the northern part of Keewatin Sector of the Laurentide Ice Sheet. A relict landscape with deeply weathered terrain was preserved under a non-erosive basal ice regime (cold-based) in the uplands south of Wager Bay; this pre-LGM landscape is atypical for mainland Nunavut and has never been documented thoroughly prior to this study. The uplands coincide with a relatively narrow and stable position of a major ice divide in Keewatin (KID) as indicated by opposing ice-flow indicators on single outcrops or the absence of any ice-flow indicators. The entire KID zone alternates between bouldery till blankets and veneers, patchy areas of weathered bedrock and diamictons, boulder fields, and felsenmeer retaining the bedrock structure. Along the southwestern shores of Wager Bay north of the ice divide, early N and NNE ice flows, as well as late NE ice flows into the bay, are observed as far as Masivak Creek, therefore confining the KID extension into the bay east of Masivak Creek. On either side of the KID central axis, swaths of streamlined bedrock and till landforms extend outward to the southeast (S to SSE) or to the north (NNW to NNE). A complex system of subglacial meltwater corridors and proglacial meltwater channels overprints the streamlined till that extends on the southward side of the KID. A later S to SSE deglacial event locally cross-cuts the streamlined terrain and corridors, as indicated by eskers, young striations and few subglacial landforms, and suggest a more northward ice margin retreat. The post-glacial marine limit increases from ~118 m asl southwest of Wager Bay near Paliak Islands to 140 m along Roes Welcome Sound and stays relatively constant at 140-150 m westward towards Tehery Lake. At the marine limit, erosion and reworking of glacial sediments have formed boulder beaches, wave-washed surfaces, terraces, glaciomarine deltas, and wave-cut notches in till. Below the marine limit, silty sandy marine veneers are scattered in low areas; boulder beaches skirt some eskers ridges or fill in embayments between bedrock outcrops along the coastal areas.

The main ice-flow trends south of the KID, varying between SSE and SE, are responsible for the most prominent streamlined landforms and the predominant directions of glacial transport in the study area. SSE trends are dominant in the western sector and towards the uplands while SE directions extend to Roes Welcome Sound in the eastern sector. Generally the late deglacial flows to the SSE in the eastern sector, parallel to late esker trends, had probably minor influence on surface till composition. NNW glacial indicators of ice-flow and glacial transport characterize the areas north of the KID.

The area has a known potential for diamondiferous kimberlite with the presence of the Nanuq kimberlite bodies in the ice divide area. Glacial erosion and transport of kimberlite debris in a SSE direction has formed a 60-km long SSE-trending regional dispersal train of multiple KIMs in regional till samples,

including a significant number of Cr-pyrope, eclogitic garnet and Ca-forsterite. Unknown kimberlite with a potential for diamonds is also suggested at Meen Lake, 180 km to the ESE of Nanuq in the Gordon domain, with the occurrence of Cr-pyrope, eclogitic garnet, Ca-forsterite, picroilmenite, low Cr-diopside and bronzite grains in a single till sample. A local source up-ice (northwest) of the sample is indicated by the preservation of a kelyphite rim on one 0.5-1 mm Cr-pyrope grain (G9); composition of olivine in this till sample ($Fo_{78-92}$) is unlike that of olivine ($Fo_{70-74}$) from the underlying coronitic ultramafic layered intrusion. Duplicating the results of this sample as well as additional sampling on the western side and up-ice of Meen Lake is recommended to confirm this potential.

The study area also has potential for Ni-Cu-PGEs and chromite. A 60 to 100 km-long SE trending fan-shaped dispersal train of Mg-rich olivine grains in till, including forsterite, reflects palimpsest glacial transport in south to southeast directions from potential sources in the Lorillard supracrustal belt. Large numbers of coarse-grained Mg-rich olivine (0.5-1mm), olivine chemistry, Pt and Pd values in till matrix and meta-komatiite pebbles in till suggest local sources of olivine-rich mantle rocks, such as peridotite bodies within the Lorillard belt. However the highest potential for Ni-Cu-PGEs-chromite mineralization lies over the heavily drift-covered eastern part of the northern Lorillard belt, with the presence of a relatively short (< 30 km) SE dispersal train of chromite grains, distinct from the Mg-rich olivine dispersal fan, and the occurrence of 5 speryllite grains in 3 samples of the same area. A local source in mafic to ultramafic bodies not yet mapped amongst the Archean tonalite to granodiorite gneiss of the Lorillard and adjacent Gordon domains is suggested here. Jefferson et al. (1991) suggested a low to moderate potential for magmatic deposits related to layered igneous rocks in the Daly Bay complex but this area was not sampled for till as part of the current study hence cannot be assessed further for mineral potential.

Finally, till composition shows the area has some potential for base- and precious metal mineralization in supracrustal rocks of the northern part of the Lorillard domain and in several other supracrustal panels north of the Chesterfield shear zone. The presence of numerous MMSIMs in a few till samples are potentially indicative of hydrothermal alteration associated with metamorphosed VMS deposits. Anomalous till samples in Cu, Ni and Zn also suggested a low to moderate potential for base metals in the supracrustal belts on either side of Wager Bay within the National Park's boundary (Jefferson et al., 1991). Potential for skarn or greisen mineralization in the Pennington supracrustal belt within the eastern part of the Douglas Harbour domain north of the Wager shear zone is indicated but remains to be determined.

## ACKNOWLEDGEMENTS

This work was conducted as part of Tehery-Wager project within the Rae Area of Interest of the GEM-2 Program. We are most grateful to Holly Steenkamp (CNGO) to help manage the field logistics in 2015 and 2016, Linda Ham (CNGO) for providing funds through SINED, and Étienne Girard for GIS support during and after the field work. In addition we gratefully acknowledge Discovery Mining Services in Yellowknife with camp logistics; Greg Tanuyak in Chesterfield Inlet and Helen Moffat and Boris Kotelewetz in Baker Lake for their expediting services, Ookpik Aviation and Prairie Helicopters (Erik Polzin) for expert fixed and rotary wing support, Louise Levesque and Debbi Guilfoyle for the most enjoyable meals, and Polar Continental Shelf Program for logistical support (Project #053-15 and #059-16). Finally we thank Tony Peterson, Chris Lawley, Vicki Tschirhart and Owen Weller (GSC colleagues), Martin Roy (UQAM), Carl Guilmette (Université Laval), Justin Byatt (UNB) and Katrina Hatogina, Jeremy Beales, Billy Garrison, Jillian Kendrick, Loraine Lebeau, Allan Lion, Ryan Bayne (bedrock field assistants)

for enthusiastic support and assistance during the surficial surveys, and bear monitors W. Angotinjoar, J. Autut, T. Evviuk and A. Alooq and assistant cook R. Issaluk. Shauna Madore (GSC-Sedimentology Laboratory), Jeanne Percival and Igor Bilot (GSC-Mineralogy) and Katherine Venance (GSC-Microbeam Laboratory) are acknowledged for till samples preparation and analysis; R. Huneault, S. Averill and the Overburden Drilling Management team are thanked for heavy mineral processing, indicator mineral picking and pebble clast analysis. Iyse Randour was supported by an NSERC grant as part of an MSc thesis at UQAM under the supervision of Dr. Martin Roy. We thank Beth McClenaghan for kindly reviewing the report.

## REFERENCES

Arndt, N.T., Guitreau, M., Boullier, A.M., Le Roex, A., Tommasi, A., Cordier, P., and Sobolev, A., 2010. Olivine and the origin of kimberlite; Journal of Petrology, v. 51, p. 573–602.

Averill, S.A., 2001. The application of heavy indicator mineralogy in mineral exploration with emphasis on base metal indicators in glaciated metamorphic and plutonic terrains; in McClenaghan, M.B., Bobrowsky, P.T., Hall, G.E.M. & Cook, S.J. (eds) Drift Exploration in Glaciated Terrain. Geological Society, London, Special Publication, 185, 69-82.

Averill, S.A. and Huneault, R., 2006. Overburden Drilling Management Ltd: Exploring heavy minerals; EXPLORE, Newsletter of the Association of Applied Geochemists, v. 133, p. 1-5.

Aylsworth, J.M., 1990a. Surficial Geology, Tehery Lake, District of Keewatin, Northwest Territories; Geological Survey of Canada, Preliminary Map 46-1989, 1:250,000 scale.

Aylsworth, J.M., 1990b. Surficial Geology, Armit Lake, District of Keewatin, Northwest Territories; Geological Survey of Canada, Preliminary Map 45-1989, 1:125,000 scale.

Aylsworth, J. M. and Shilts, W. W., 1989. Glacial features around the Keewatin Ice divide: Districts of MacKenzie and Keewatin; Geological Survey of Canada, Paper 88-24, 21 p.

Boulton, G.S. and Clark, C.D., 1990. A highly mobile Laurentide ice sheet revealed by satellite images of glacial lineations; Nature, v. 346, p. 813-817.

Bussweiler, Y., Brey, G.P., Pearson, D.G., Stachel, T., Stern, R.A., Hardman, M.F., Kjarsgaard, B.A., and Jackson S.E., 2017. The aluminum-in-olivine thermometer for mantle peridotites - Experimental versus empirical calibration and potential applications; Lithos, v. 272–273, p. 301-314.

Byatt, J., 2017. Mapping surficial materials in Nunavut using RADARSAT-2 C-HH and C-HV, Landsat-8 OLI, DEMand slope data; MSc Thesis, Graduate Academy Unit of Forestry and Environmental Management, University of New Brunswick, Fredericton, 97 pages.

Byatt, J., LaRocque, A., Leblon, B., McMartin, I., and Harris, J. 2015. Mapping surficial materials south of Wager Bay, southern Nunavut, using RADARSAT-2 C-band dual-polarized and Landsat 8 images, a digital elevation model and slope data: preliminary map and summary of fieldwork; Summary of Activities 2015, Canada-Nunavut Geoscience Office, p. 135–144.

Byatt, J., LaRocque, A., and Leblon, B., 2016. Mapping surficial materials north of Wager Bay, Nunavut, using RADARSAT-2 C-HH and C-HV, Landsat-8 OLI, DEM and slope data; in Book of Abstracts, Canadian Association of Geographers 2016 Conference, Halifax, Nova Scotia, p. 91.

Byatt, J., LaRocque, A., Leblon, B., Harris, J. and McMartin, I., 2019a. Mapping Surficial Materials in Nunavut Using RADARSAT-2 coulombs-HH and C-HV, Landsat-8 OLI, DEM and Slope Data; Canadian Journal of Remote Sensing, v. 44, p. 491-512.

Byatt, J., LaRocque, A., Leblon, B., Harris, J. and McMartin, I., 2019b. Mapping Surficial Materials in south of Wager Bay area (Nunavut) using RADARSAT-2 C-HH and C-HV, Landsat-8 OLI, DEM and slope data; International Journal of Earth & Environmental Sciences, v. 4, IJEES-164.

Clark, C.D., 1997. Reconstructing the evolutionary dynamics of former ice-sheets using multi-temporal evidence, remote sensing and GIS; Quaternary Science Reviews, v. 16, p. 1067-1092.

Corrigan, D., Nadeau, L., Brouillette, P., Wodicka, N., Houlé, M.G., Tremblay, T., Machado, G., and Keating, P., 2013. Overview of GEM Multiple Metals – Melville Peninsula project, central Melville Peninsula, Nunavut. Geological Survey of Canada, Current Research 2013-19, 17 p.

Coulthard, R.D., Furze, M.F.A., Pienkowski, A.J., Chantel Nixon, F., England, J.H., 2010. New marine DR values for Arctic Canada; Quaternary Geochronology, v. 5, p. 419-434.

Craig, B.G., 1965. Notes on moraines and radiocarbon dates in Northwest Baffin Island, Melville Peninsula, and Northeast District of Keewatin; Geological Survey of Canada, Paper 65-20, 7 p.

Day, S.J.A., Wodicka, N., and McMartin, I., 2013. Preliminary geochemical, mineralogical and indicator mineral data for heavy mineral concentrates and waters, Lorillard River area, Nunavut (parts of NTS 056 A, B and G); Geological Survey of Canada, Open File 7428, 11 p.

De Angelis, H., 2007. Glacial geomorphology of the east-central Canadian Arctic; Journal of map, v. 3, p. 323-341.

De Angelis, H. and Kleman, J., 2005. Palaeo-ice streams in the northern Keewatin sector of the Laurentide ice sheet; Annals of Glaciology, v. 42, p. 135-144.

De Angelis, H. and Kleman, J., 2007. Palaeo-ice streams in the Foxe/Baffin sector of the Laurentide Ice Sheet; Quaternary Science Reviews, v. 26, p. 1313-1331.

De Angelis, H. and Kleman, J., 2008. Palaeo-ice-stream onsets; examples from the north-eastern Laurentide ice sheet; Earth Surface Processes and Landforms, v. 33, p. 560-572.

Dredge, L.A. and McMartin, I., 2005. Postglacial marine deposits and marine limit determinations, inner Wager Bay area, Kivalliq region, Nunavut; Geological Survey of Canada, Current Research no. 2005-B3, 5 p.

Dredge, L.A., McMartin, I., and Ford, K., 2005. Till geochemistry, gamma ray spectrometry, and gold grain counts, Wager Bay area, mainland Nunavut (NTS 56 G); Geological Survey of Canada, Open File 5014.

Dredge, L.A., McMartin, I. and Kjarsgaard, I.M., 2006. Kimberlite indicator minerals in till from the Wager Bay area, mainland Nunavut: data and interpretation (NTS 56G); Geological Survey of Canada, Open File 5087.

Dredge, L.A. and McMartin, I., 2007. Surficial geology, Wager Bay, Nunavut; Geological Survey of Canada, "A" Series Map 2111A, 1:250,000 scale.

Dredge, L.A., McMartin, I., and Campbell, J.E., 2013a. Reconnaissance surficial geology, Yellow Bluff (west), Nunavut, NTS 46D, West; Geological Survey of Canada, CGM map 145, 1:100,000 scale.

Dredge, L.A., McMartin, I., and Campbell, J.E., 2013b. Reconnaissance surficial geology, Daly Bay (south) and Cape Fullerton (north), Nunavut, NTS 56-A, South and 55-P, North; Geological Survey of Canada, CGM map 146, 1:100,000 scale.

Dredge, L.A., McMartin, I., and Campbell, J.E., 2013c. Reconnaissance surficial geology, Daly Bay (north), Nunavut, NTS 56-A, North; Geological Survey of Canada, CGM map 147, 1:100,000 scale.

Dyke, A.S., 2004. An outline of North American deglaciation with emphasis on central and northern Canada; In: J. Ehlers and P.L. Gibbard, eds., Quaternary Glaciations: Extent and Chronology, Part II. Elsevier, Amsterdam, p. 373-424.

Dyke, A. S. and Prest, V. K., 1987. Late Wisconsinan and Holocene history of the Laurentide Ice Sheet; Géographie physique et Quaternaire, v. 41, p. 237-263.

Dyke, A.S., Moore, A. and Robertson, L., 2003. Deglaciation of North America; Geological Survey of Canada, Open File 1574.

Fipke, C.E., Gurney, J.J. and Moore, R.O., 1995. Diamond exploration techniques emphasizing indicator mineral geochemistry and Canadian examples; Geological Survey of Canada, Bulletin 423, 86 p.

Foley, S.F., Andronikov, A.V., Jacob, D.E., and Melzer, S., 2006. Evidence from Antarctic mantle peridotite xenoliths for changes in mineralogy, geochemistry and geothermal gradients beneath a developing rift; Geochim. Cosmochim. Acta, v. 70, p. 3096-3120.

Garrett, R.G., 1983. Sampling Methodology; *in* Statistics and Data Analysis in Geochemical Prospecting, Handbook of Exploration Geochemistry, Vol. 2, R.J. Howarth (G.J.S. Govett, series ed), Elsevier, Amsterdam, Chapter 4, p. 83-110.

Garrison, W., 2016. Geology of a Metasedimentary Package in the Outer Shear Zone of the Daly Bay Complex, Central Nunavut. B.Sc. research project, Dalhousie University, Halifax, Nova Scotia, 36 p.

Girard, I, Klassen, R.A. and Laframboise, R.R., 2004. Sedimentology laboratory manual, Terrain Sciences Division; Geological Survey of Canada, Open File 4823.

Gordon, T.M., 1988. Precambrian Geology of the Daly Bay Area, District of Keewatin; Geological Survey of Canada, Memoir 422, 21 pages.

Gosse, J.C. and Phillips, F.M., 2001. Terrestrial in situ cosmogenic nuclides: theory and application; Quaternary Science Reviews, v. 20, p. 1475-1560.

Grunsky, E.C., 2010. The interpretation of geochemical survey data; Geochemistry: Exploration, Environment, Analysis, v. 10, p. 27-74.

Hanmer, S. and Williams, M.L., 2001. Targeted fieldwork in the Daly Bay Complex, Hudson Bay, Nunavut; Geological Survey of Canada, Current Research no. 2001-C15, 24 p.

Hinchey, A., Davis, W.J., Ryan, J.J., and Nadeau, L., 2011. Neoarchean high potassium granites of the Boothia mainland area, Rae craton, Churchill Province: U-Pb zircon and Sm-Nd whole-rock isotopic constraints; Canadian Journal of Earth Sciences, v. 48(2), p. 247–279.

Hoffman, P.F., 1990. Subdivision of the Churchill province and extent of the Trans-Hudson Orogen. In: The Early Proterozoic Trans-Hudson Orogen of North America, J.F. Lewry and M.R. Stauffer (ed.), Geological Association of Canada, Special Paper 37, p. 15–39.

Jefferson, C.W., Smith, J.E.M. and Hamilton, S.M., 1991. Preliminary Account of the Resource Assessment Study of Proposed National Park, Wager Bay - Southampton Island Areas, District of Keewatin; Geological Survey of Canada, Open File 2351.

Kleman, J., Fastook, J. and Stroeven, A.P., 2002. Geological and geomorphologically constrained numerical model of Laurentide Ice Sheet inception and build-up; Quaternary International, v. 95-96, p. 87-98.

Kleman, J., Jansson, K.N., De Angelis, H., Stroeven, A.P., Hättestrand, C., Alm, G. and Glasser, N.F., 2010. North American Ice Sheet build-up during the last glacial cycle, 115–21 kyr; Quaternary Science Reviews, v. 29, p. 2036-2051.

Kohler,T. and Brey, G.P., 1990. Ca-exchange between olivine and clinopyroxene as a geothermobarometer calibrated from 2 to 60 kbar in primitive natural lherzolites; Geochemica et Cosmochimica Acta, v. 54, p. 2375-2388.

LeCheminant, A.N. and Heaman, L.M., 1989. Mackenzie igneous events, Canada: Middle Proterozoic hotspot magmatism associated with ocean opening; Earth and Planetary Science Letters, v. 96, p. 38–48.

Lee, H.A., Craig, B.G. and Fyles, J.G., 1957. Keewatin Ice Divide; Geological Society of America, Bulletin 68, p. 1760-1761.

Lewry, J.F. and Collerson, K.D., 1990. The Trans-Hudson Orogen: extent, subdivisions and problems. In: The Early Proterozoic Trans-Hudson Orogen of North America, J.F. Lewry and M.R. Stauffer (ed.), Geological Association of Canada, Special Paper 37, p. 1–14.

Margold M., Stokes C.R. and Clark C.D., 2015. Ice streams in the Laurentide Ice Sheet: a new mapping inventory; Earth-Science Reviews, v. 143, p. 117-146.

Margold, M., Stokes, C.R., and Clark, C.D., 2018. Reconciling records of ice streaming and ice margin retreat to produce a palaeogeographic reconstruction of the deglaciation of the Laurentide Ice Sheet; Quaternary Science Reviews, v. 189, p. 1-30.

Marquette, G.C., Gray, J.T., Gosse, J.C., Courchesne, F., Stockli, L., Macpherson, G. and Finkel, R., 2004. Felsenmeer persistence under non-erosive ice in the Torngat and Kaumajet mountains, Quebec and Labrador, as determined by soil weathering and cosmogenic nuclide exposure dating; Canadian Journal of Earth Sciences, v. 41, p. 19-38.

McClenaghan, M.B., Plouffe, A., McMartin, I., Campbell, J.E., Spirito, W.A., Paulen, R.C., Garrett, R.G., and Hall, G.E.M., 2013. Till sampling and geochemical analytical protocols used by the Geological Survey of Canada; Geochemistry, Exploration, Environment, Analysis, v. 13, p. 285-301.

McClenaghan, M.B., and Kjarsgaard, B.A., 2007. Indicator mineral and surficial geochemical exploration methods for kimberlite in glaciated terrain: Examples from Canada. In: W.D. Goodfellow (Ed.), Mineral Deposits of Canada: A Synthesis of Major Deposit-Types, District Metallogeny, the Evolution of Geological Provinces, and Exploration Methods. Geological Association of Canada, Mineral Deposits Division, Special Publication No. 5, p. 983-1006.

McCurdy, M.W. and McMartin, I., 2017. Geochemical and Mineralogical Data for Stream Sediment and Proximal Till Sites, Ellice River Area, Nunavut (Parts of NTS 76-H and NTS 76-I); Geological Survey of Canada, Open File 8302.

McMartin, I., 2017. Till provenance across the terminus of the Dubawnt Lake Ice Stream, central Nunavut; Geological Survey of Canada, Current Research 2017-1, 13 p.

McMartin, I. and Henderson, P.J., 2004. Evidence from Keewatin (Central Nunavut) for paleo-ice divide migration; Géographie physique et Quaternaire, v. 58, p. 163-187.

McMartin, I., and Dredge, L.A., 2005. History of ice flow in the Shultz Lake and Wager Bay areas, Kivalliq Region, Nunavut; Geological Survey of Canada Current Research, 2005-B2, 10 p.

McMartin, I., Wodicka, N., Bazor, D., and Boyd, B., 2013. Till composition across the Rae craton south of Wager Bay, Nunavut: results from the Geo-mapping Frontiers' Tehery-Cape Dobbs project; Geological Survey of Canada, Open File 7417.

McMartin, I. Byatt, J. Randour, I., and Day, S.J.A., 2015a. Report of 2015 activities for regional surficial mapping, till and stream sediment sampling in the Tehery-Wager GEM 2 Rae Project area; Geological Survey of Canada, Open File 7966.

McMartin, I., Randour, I., Byatt, J., Roy, M., LaRocque, A., Leblon, B., Day, S., Steenkamp, H.M., and Wodicka, N., 2015b. Overview of surficial geology activities in the Tehery-Wager GEM-2 Rae Project area, Nunavut; In: Irwin, D., Normandeau, P.X. and Gervais, S.D. (compilers), 43rd Annual Yellowknife Geoscience Forum Abstracts, Northwest Territories Geological Survey, Yellowknife, NT, p. 133-134.

McMartin, I., Campbell, J.E., Dredge, L.A., LeCheminant, A.N., McCurdy, M.W., and Scromeda, N., 2015c. Quaternary geology and till composition north of Wager Bay, Nunavut: results from the GEM Wager Bay Surficial Geology Project; Geological Survey of Canada, Open File 7748.

McMartin, I., Randour, I., Byatt, J., Roy, M., LaRocque, A., Leblon, B., Day, S., Steenkamp, H.M., and Wodicka, N., 2016a. Overview of surficial geology activities in the Tehery-Wager GEM2 Rae Project area, Nunavut;

Geological Survey of Canada, Scientific Presentation No. 40.
McMartin, I., Day, S.J.A., Randour, I., Roy, M., Byatt, J., LaRocque, A., and Leblon, B., 2016b. Report of 2016 activities for surficial mapping and sampling surveys in the Tehery-Wager GEM-2 Rae Project area; Geological Survey of Canada, Open File 8134.
McMartin, I., Day, S.J.A., Randour, I., Roy, M., Steenkamp, H.M., and Wodicka, N., 2016c. Surficial geology studies across the Keewatin Ice divide, Tehery-Wager Geoscience Project area, Nunavut; In: Irwin, D., Gervais, S.D. and Terlaky, V. (compilers), 44th Yellowknife Geoscience Forum Abstracts Volume 2016, Northwest Territories Geological Survey, Yellowknife, p. 93-94.
Mills, A., Berman, R.G., Davis, W.J., Tella, S., Carr, S.D., Roddick, C., and Hanmer, S., 2007. Thermobarometry and geochronology of the Uvauk Complex: A polymetamorphic Neoarchean and Paleoproterozoic segment of the Snowbird tectonic zone, Nunavut, Canada: Canadian Journal of Earth Sciences, v. 44, p. 245–266.
Nowicki, T.E., Moore, R.O., Gurney, J.J. and Baumgartner, M.C., 2007. Diamonds and associated heavy minerals in kimberlite: a review of key concepts and applications; Developments in Sedimentology, v. 58, p. 1235–1267.
Pell, J., 2008. Technical report on the Nanuq property, Kivalliq region, Nunavut: http://www.pdiam.com/i/pdf/Nanuq-43-101-2008.pdf.
Pell, J.A. and Strickland, D., 2004. Assessment report on indicator mineral sampling on the Nanuq property, Kivalliq Region, Nunavut, Dunsmuir Ventures Ltd. Indigenous and Northern Affairs Canada, Assessment Report 084756, 89 p.
Pehrsson, S., Berman, R.G., and Davis, W.J., 2013. Paleoproterozoic orogenesis during Nuna aggregation: a case study of reworking of the Rae craton, Woodburn Lake, Nunavut. Precambrian Research, v. 232, p. 167–188.
Peterson, T.D., van Breemen, O., Sandeman, H., Cousens, B., 2002. Proterozoic (1.85-1.75 Ga) igneous suites of the Western Churchill Province: granitoid and ultrapotassic magmatism in a reworked Archean hinterland. Precambrian Research, v. 119, p. 73-100.
Peterson, T.D., Jefferson, C.W., Anand, A., 2015. Geological setting and geochemistry of the ca. 2.6 Ga Snow Island Suite in the central Rae Domain of the Western Churchill Province, Nunavut. Geological Survey of Canada Open File 7841.
Peterson, T.D., Wodicka, N., Steenkamp, H., and Tschirhart, V., in prep. Lithogeochemical and Sm-Nd Isotopic Data for the Tehery-Wager Region, Nunavut, 2015-2017; Geological Survey of Canada, Open File.
Plouffe, A., McClenaghan, M.B., Paulen, R.C., McMartin, I., Campbell, J., and Spirito, W., 2013a. Processing of unconsolidated glacial sediments for the recovery of indicator minerals: protocols used at the Geological Survey of Canada; Geochemistry, Exploration, Environment, Analysis, v. 13, p. 303-316.
Plouffe, A., McClenaghan, M.B., Paulen, R.C., McMartin, I., Campbell, J.E., and Spirito, W.A., 2013b. Quality assurance and quality control measures applied to indicator mineral studies at the Geological Survey of Canada; in New frontiers for exploration in glaciated terrain, Paulen, R.C. and McClenaghan, M.B. (eds.), Geological Survey of Canada, Open File Report 7374, p. 13-19.
Prest, V.K., Grant, D.R., and Rampton, V.N., 1968. Glacial Map of Canada; Geological Survey of Canada, Map 1253A, Scale 1:5 000 000.
Rainbird, R.H., Davis, W.J., Pehrsson, S.J., Wodicka, N., Skulski, T., 2010. Early Paleoproterozoic supracrustal assemblages of the Rae domain, Nunavut, Canada: intracratonic basin development during supercontinent break-up and assembly; Precambrian Research, v. 181, p. 167–186.
Randour, I., 2018. Géologie Quaternaire de la région de Wager Bay, Nunavut: cartographie, datation de rivages marins et impacts de l'invasion marine sur la géochimie des sédiments glaciaires; Mémoire de maîtrise, Département des Sciences de la Terre et de l'atmosphère, UQÀM, Montréal, 144 p.
Randour, I., Roy, M., and McMartin, I., 2016a. Glacial dynamics and deglaciation of Wager Bay: Implication for drift prospecting; Congrès des étudiants du Géotop 2016, Montréal, 19-20 mars 2016, poster.
Randour, I., McMartin, I., and Roy, M., 2016b. Study of the postglacial marine limit between Wager Bay and Chesterfield Inlet, western Hudson Bay, Nunavut; in Summary of Activities 2016, Canada-Nunavut Geoscience Office, p. 51–60.
Randour, I. and McMartin, I., 2017. Surficial geology, Douglas Harbour (south), Nunavut, NTS 56-H south; Geological Survey of Canada, Canadian Geoscience Map 312, (ed. prelim.), scale 1:100 000, 1 sheet.
Randour, I., Roy, M., McMartin, I., and Schaefer, J.M., 2017a. Maximum extent and chronology of the postglacial Tyrrell Sea in Northwestern Hudson Bay, Nunavut; Congrès des étudiants du Géotop 2017, Rimouski, 19-20 mars 2017, poster.
Randour, I., McMartin, I., and Roy, M., 2017b. Effects of marine inundation on till composition in permafrost terrain South of Wager Bay, central Mainland Nunavut; Kingston 2017: GAC-MAC Joint Annual Meeting, Kingston, Ontario, Program with abstracts, Volume 40, p. 323.
Randour, I., Dredge, L.A., McMartin, I. and Campbell, J.E., in press. Surficial geology, Cape Dobbs, Nunavut, NTS 46-E; Geological Survey of Canada, Canadian Geoscience Map, scale 1:100 000, 1 sheet.

Randour, I., Roy, M., McMartin, I. and Schaefer, J.M., in prep-1. Extent and chronology of the Tyrrell Sea incursion in northwestern Hudson Bay (Canada) based on the mapping and cosmogenic $^{10}$Be dating of raised marine landforms; paper in preparation for submission to Boreas.

Randour, I., McMartin, I., and Roy, M., in prep-2. Effects of marine processes on till composition near the marine limit south of Wager Bay, central Mainland Nunavut; paper in preparation for submission to GSC Current Research or GEEA.

Reimer, P.J., Bard, E., Bayliss, A., Beck, J.W., Blackwell, P.G., Bronk Ramsey, C., Buck, C.E., Cheng, H., Edwards, R.L., Friedrich, M., Grootes, P.M., Guilderson, T.P., Haflidason, H., Hajdas, I., Hatté, C., Heaton, T.J., Hogg, A.G., Hughen, K.A., Kaiser, K.F., Kromer, B., Manning, S.W., Niu, M., Reimer, R.W., Richards, D.A., Scott, E.M., Southon, J.R., Turney, C.S.M., and van der Plicht, J., 2013. IntCal13 and MARINE13 radiocarbon age calibration curves 0-50000 years calBP; Radiocarbon, v. 55, p. 1869-1887.

Refsnider K.A and Miller G.H., 2010. Reorganization of ice sheet flow patterns in arctic Canada and the mid-Pleistocene transition. Geophysical Research Letters, v. 37, L13502.

Sanborn-Barrie, M., Davis, W.J., Berman, R.G., Rayner, N., Skulski, T., Sandeman, H.A., 2014. Neoarchean continental crust formation and Paleoproterozoic deformation of the central Rae craton, Committee Bay belt, Nunavut; Canadian Journal of Earth Sciences, v. 51, p. 635–667.

Skulski, T., Sanborn-Barrie, M., Sandeman, H.A., 2003. Geology: Walker Lake and Arrowsmith River area, Nunavut; Geological Survey of Canada, Open File 3777 (1:100,000 scale, 2 sheets).

Smith, J.E.M. 1990. The glacial history of the Wager Bay area, District of Keewatin, N.W.T.; unpublished M. Sc. Thesis, Carleton University, Ottawa, 107 p.

Steenkamp, H.M., Wodicka, N., Lawley, C.J.M., Peterson, T.D., and Guilmette, C., 2015. Overview of bedrock mapping and results from portable X-ray fluorescence spectrometry in the eastern part of the Tehery Lake–Wager Bay area, western Hudson Bay, Nunavut; in Summary of Activities 2015, Canada-Nunavut Geoscience Office, p. 121–134.

Steenkamp, H.M., Wodicka, N., Weller, O.M., and Kendrick, J., 2016. Overview of bedrock mapping in the northern and western parts of the Tehery Lake–Wager Bay area, western Hudson Bay, Nunavut; in Summary of Activities 2016, Canada-Nunavut Geoscience Office, p. 27–39.

Steenkamp, H.M., Wodicka, N., Guilmette, C., Lawley, C.J.M, and Weller, O.M., 2017. Supracrustal rocks of the Tehery-Wager area: Distinct packages and their metamorphic assemblages; Kingston 2017: Geological Association of Canada-Mineralogical Association of Canada, Kingston, Ontario, Program with abstracts, v. 40, p. 359.

Stuiver, M., Reimer, P.J., Reimer, R.W., 2018. CALIB 7.1 [WWW program] at http://calib.org, accessed 2018-3-6.

Spirito, W.A., McClenaghan, M.B., Plouffe, A., McMartin, I., Campbell, J.E., Paulen, R.C., Garrett, R.G. and Hall, G.E.M., 2011. Till Sampling and Analytical Protocols for GEM Projects: from field to archive; Geological Survey of Canada Open File 6850.

Tschirhart, V.L., Wodicka, N., and Steenkamp, H.M., 2016. Shallow crustal structure of the Tehery Lake–Wager Bay area, western Hudson Bay, Nunavut, from potential-field datasets; in Summary of Activities 2016, Canada-Nunavut Geoscience Office, p. 41–50.

Thomas, R. and Dyke, A.S., 1981. Surficial geology, Pennington Lake, District of Keewatin, Northwest Territories; Geological Survey of Canada, Preliminary Map 4-1981, 1:250,000 scale.

van Breemen, O., Peterson, T.D., Sandeman, H.A., 2005. U-Pb zircon geochronology and Nd isotope geochemistry of Proterozoic granitoids in the western Churchill Province: intrusive age pattern and Archean source domains. Canadian Journal of Earth Sciences, v. 42, p. 339-377.

Wodicka, N., Steenkamp, H.M., Lawley, C.J.M., Peterson, T.D., Guilmette, C., Girard, É., and Buenviaje, R., 2015. Report of 2015 activities for the bedrock geology and economic potential of the Tehery-Wager area: GEM-2 Rae Project. Geological Survey of Canada Open File 7970.

Wodicka, N., Steenkamp, H.M., Weller, H.M., Kendrick, J., Tschirhart, V.L., Peterson, T.D., and Girard, É., 2016a. Report of 2016 activities for the geology and economic potential of the Tehery-Wager area: GEM-2 Rae Project. Geological Survey of Canada Open File 8149.

Wodicka, N., Steenkamp, H.M., McMartin, I., Day, S., Lawley, C.J.M., Peterson, T., Whalen, J., Guilmette, C., Tschirhart, V., and Garrison, W., 2016b. Geology and Mineral Potential of the Tehery-Wager area, Nunavut: Highlights from a GEM-2 Rae activity; Nunavut Mining Symposium, Iqaluit, April 2016, https://numining.squarespace.com/s/4-Wodicka-GSC.pdf.

Wodicka, N., Steenkamp, H.M., Peterson, T.D., McMartin, I., Day, S.J.A., and Tschirhart, V.L., 2017a. Report of 2017 activities for the geology and economic potential of the Tehery-Wager area: GEM-2 Rae Project; Geological Survey of Canada Open File 8318.

Wodicka, N., Steenkamp, H.M., Peterson, T., Whalen J., and Lawley, C.J.M., 2017b. Neoarchean to Paleoproterozoic evolution of the south-central Rae margin, Tehery-Wager area, Nunavut: Insights from field mapping, U-Pb

geochronology, and Sm-Nd isotope data; Kingston 2017: Geological Association of Canada-Mineralogical Association of Canada, Kingston, Ontario, Program with abstracts, v. 40, p. 423.

Wodicka, N., Whalen, J.B., Kellett, D.A., Harris, J.R., Berman, R.G., Ferderber, J.L., Girard, É., Hillary, E.M., Buenviaje, R., Bazor, D., Joseph, J., Sandeman, H.A., and Davis, W.J., in prep. Bedrock geology across the Rae craton south of Wager Bay, Nunavut: results from the Geo-mapping Frontiers' Tehery-Cape Dobbs project; Geological Survey of Canada, Open File.

Wyatt, B.A., Baumgartner, M., Anckar, E., Grütter, H.S., 2004. Compositional classification of ''kimberlitic'' and "non-kimberlitic" ilmenite; Lithos, v. 77, p. 819–840.

Zheng, J.P., Griffin, W.L., O'Reilly, S.Y., Yang, J.S., Li, T.F., Zhang, M.,Zhang, R.Y., and Liou, J.G., 2006. Mineral chemistry of peridotites from Paleozoic, Mesozoic and Cenozoic lithosphere: constraints on mantle evolution beneath eastern China; J. Petrol., v. 47, p. 2233–2256.